References

1 Parkin DM, Bray F, Ferlay J, Pisani P. Global cancer statistics, 2002. *CA Cancer J. Clin.* 2005; **55**: 74–108.
2 Bruix J, Sherman M. Management of hepatocellular carcinoma. *Hepatology* 2005; **42**: 1208–36.
3 Rossi S, Di Stasi M, Buscarini E *et al.* Percutaneous RF interstitial thermal ablation in the treatment of hepatic cancer. *AJR Am. J. Roentgenol.* 1996; **167**: 759–68.
4 Livraghi T, Goldberg SN, Lazzaroni S, Meloni F, Solbiati L, Gazelle GS. Small hepatocellular carcinoma: treatment with radio-frequency ablation versus ethanol injection. *Radiology* 1999; **210**: 655–61.
5 Shiina S, Teratani T, Obi S *et al.* A randomized controlled trial of radiofrequency ablation with ethanol injection for small hepatocellular carcinoma. *Gastroenterology* 2005; **129**: 122–30.
6 Ikai I, Arii S, Okazaki M *et al.* Report of the 17th nationwide follow-up survey of primary liver cancer in Japan. *Hepatol. Res.* 2007; **37**: 676–91.
7 Tanaka S, Kitamura T, Nakanishi K, Okuda S, Kojima J, Fujimoto I. Recent advances in ultrasonographic diagnosis of hepatocellular carcinoma. *Cancer* 1989; **63**: 1313–7.
8 Nakai M, Sato M, Sahara S *et al.* Radiofrequency ablation assisted by real-time virtual sonography and CT for hepatocellular carcinoma undetectable by conventional sonography. *Cardiovasc Intervent Radiol.* 2009; **32**: 62–9.
9 Sato M, Watanabe Y, Tokui K, Kawachi K, Sugata S, Ikezoe JC. T-guided treatment of ultrasonically invisible hepatocellular carcinoma. *Am. J. Gastroenterol.* 2000; **95**: 2102–6.
10 Fujimoto M, Moriyasu F, Nishikawa K, Nada T, Okuma M. Color Doppler sonography of hepatic tumors with a galactose-based contrast agent: correlation with angiographic findings. *AJR Am. J. Roentgenol.* 1994; **163**: 1099–104.
11 Kudo M, Tomita S, Tochio H *et al.* Sonography with intraarterial infusion of carbon dioxide microbubbles (sonographic angiography): value in differential diagnosis of hepatic tumors. *AJR Am. J. Roentgenol.* 1992; **158**: 65–74.
12 Kudo M. New sonographic techniques for the diagnosis and treatment of hepatocellular carcinoma. *Hepatol. Res.* 2007; **37** (Suppl. 2): S193–9.
13 Moriyasu F, Itoh K. Efficacy of perflubutane microbubble-enhanced ultrasound in the characterization and detection of focal liver lesions: phase 3 multicenter clinical trial. *AJR Am. J. Roentgenol.* 2009; **193**: 86–95.
14 Numata K, Morimoto M, Ogura T *et al.* Ablation therapy guided by contrast-enhanced sonography with Sonazoid for hepatocellular carcinoma lesions not detected by conventional sonography. *J. Ultrasound Med.* 2008; **27**: 395–406.
15 Minami Y, Kudo M, Hatanaka K *et al.* Radiofrequency ablation guided by contrast harmonic sonography using perfluorocarbon microbubbles (Sonazoid) for hepatic malignancies: an initial experience. *Liver Int.* 2010; **30**: 759–64.
16 Torzilli G, Minagawa M, Takayama T *et al.* Accurate preoperative evaluation of liver mass lesions without fine-needle biopsy. *Hepatology* 1999; **30**: 889–93.
17 Edmondson HA, Steiner PE. Primary carcinoma of the liver: a study of 100 cases among 48 900 necropsies. *Cancer* 1954; **7**: 462–503.
18 Tateishi R, Shiina S, Teratani T *et al.* Percutaneous radiofrequency ablation for hepatocellular carcinoma. An analysis of 1000 cases. *Cancer* 2005; **103**: 1201–9.
19 Tanimoto A, Yuasa Y, Shinmoto H *et al.* Superparamagnetic iron oxide-mediated hepatic signal intensity change in patients with and without cirrhosis: pulse sequence effects and Kupffer cell function. *Radiology* 2002; **222**: 661–6.
20 Kondo Y, Yoshida H, Tateishi R, Shiina S, Kawabe T, Omata M. Percutaneous radiofrequency ablation of liver cancer in the hepatic dome using the intrapleural fluid infusion technique. *Br. J. Surg.* 2008; **95**: 996–1004.
21 Kondo Y, Yoshida H, Shiina S, Tateishi R, Teratani T, Omata M. Artificial ascites technique for percutaneous radiofrequency ablation of liver cancer adjacent to the gastrointestinal tract. *Br. J. Surg.* 2006; **93**: 1277–82.

Research Article

EASL EUROPEAN ASSOCIATION FOR THE STUDY OF THE LIVER | JOURNAL OF HEPATOLOGY

Pathogenesis of lipid metabolism disorder in hepatitis C: Polyunsaturated fatty acids counteract lipid alterations induced by the core protein

Hideyuki Miyoshi[1], Kyoji Moriya[1], Takeya Tsutsumi[1], Seiko Shinzawa[1], Hajime Fujie[1], Yoshizumi Shintani[1], Hidetake Fujinaga[1], Koji Goto[1], Toru Todoroki[2], Tetsuro Suzuki[3], Tatsuo Miyamura[3], Yoshiharu Matsuura[4], Hiroshi Yotsuyanagi[1], Kazuhiko Koike[1,*]

[1]*Department of Internal Medicine, Graduate School of Medicine, University of Tokyo, Tokyo, Japan;* [2]*Department of Laboratory Medicine, Keio University School of Medicine, Tokyo, Japan;* [3]*Department of Virology II, National Institute of Infectious Diseases, Tokyo, Japan;* [4]*Department of Molecular Virology, Research Institute for Microbial Diseases, Osaka University, Osaka, Japan*

Background & Aims: Disturbance in lipid metabolism is one of the features of chronic hepatitis C, being a crucial determinant of the progression of liver fibrosis. Experimental studies have revealed that the core protein of hepatitis C virus (HCV) induces steatosis.

Methods: The activities of fatty acid metabolizing enzymes were determined by analyzing the fatty acid compositions in HepG2 cells with or without core protein expression.

Results: There was a marked accumulation of triglycerides in core-expressing HepG2 cells. While the oleic/stearic acid (18:1/18:0) and palmitoleic/palmitic acid ratio (16:1/16:0) were comparable in both the core-expressing and the control cells, there was a marked accumulation of downstream product, 5,8,11-eicosatrienoic acid (20:3(n-9)) in the core-expressing HepG2 cells. The addition of eicosatetraynoic acid, which inhibits delta-6 desaturase activity which is inherently high in HepG2 cells, led to a marked accumulation of oleic and palmitoleic acids in the core-expressing cells, showing that delta-9 desaturase was activated by the core protein. Eicosapentaenoic acid (20:5(n-3)) or arachidonic acid (20:4(n-6)) administration significantly decreased delta-9 desaturase activity, the concentration of 20:3(n-9), and triglyceride accumulation. This lipid metabolism disorder was associated with NADH accumulation due to mitochondrial dysfunction, and was reversed by the addition of pyruvate through NADH utilization.

Conclusions: The fatty acid enzyme, delta-9 desaturase, was activated by HCV core protein and polyunsaturated fatty acids counteracted this impact of the core protein on lipid metabolism. These results may open up new insights into the mechanism of lipid metabolism disorder associated with HCV infection and provide clues for the development of new therapeutic devices.

Keywords: Steatosis; Oleic acid; Core protein; Lipid metabolism; Desaturase; Hepatocellular carcinoma; NADH.

Received 31 March 2010; received in revised form 8 June 2010; accepted 5 July 2010; available online 22 September 2010

* Corresponding author. Address: Department of Gastroenterology, Graduate School of Medicine, University of Tokyo, 7-3-1 Hongo, Bunkyo-ku, Tokyo 113-8655, Japan. Tel.: +81 3 5800 8800; fax: +81 3 5800 8799.

E-mail address: kkoike-tky@umin.ac.jp (K. Koike).

Abbreviations: HCV, hepatitis C virus; HCC, hepatocellular carcinoma; PUFA, polyunsaturated fatty acids; PPAR, peroxisome proliferators-activated receptors; SREBP, sterol regulatory element binding protein; EPA, eicosapentaenoic acid; AA, arachidonic acid; ETYA, eicosatetraynoic acid; NADH, nicotinamide adenine dinucleotide; KBR, ketone body ratio.

Introduction

Persistent hepatitis C virus (HCV) infection leads to the development of chronic hepatitis, cirrhosis, and eventually, hepatocellular carcinoma (HCC), thereby being a serious problem worldwide both in medical and in socio-economical settings [1]. Histologically, several distinct features, such as bile duct damage, lymphoid follicle formation, and steatosis, (fatty change) characterize chronic hepatitis C [2–4]. Among these, steatosis is reproducible in experimental systems, both *in vitro* and *in vivo*, in which HCV proteins, particularly the core protein of HCV, are expressed. The introduced core gene induces the formation of lipid droplets in the cytoplasm of cultured cells [5,6], and in transgenic mice, it induces hepatic steatosis resembling that in chronic hepatitis C patients [7–10].

In addition, evidence has accumulated showing that steatosis is a crucial determining factor for the progression of liver fibrosis [11–13]. Steatosis and serum lipid profiles are also associated with sustained virological response to ribavirin/interferon combination therapy [14,15]. Moreover, HCV transgenic mice resemble chronic hepatitis C patients in terms of the development of HCC, implying that the HCV core protein is one of the most important viral molecules in the pathogenesis of hepatitis C [16,17]. It would thus be meaningful to explore the precise role of the core protein in modulating lipid metabolism, which may also be involved in hepatocarcinogenesis. More recently, involvement of the metabolism of lipids such as sphingolipids or cholesterol has been implicated in the replication of HCV, with a formation of lipid rafts, which are considered to be the place for HCV replication [18,19], hereby highlighting again the importance of lipid metabolism in HCV infection.

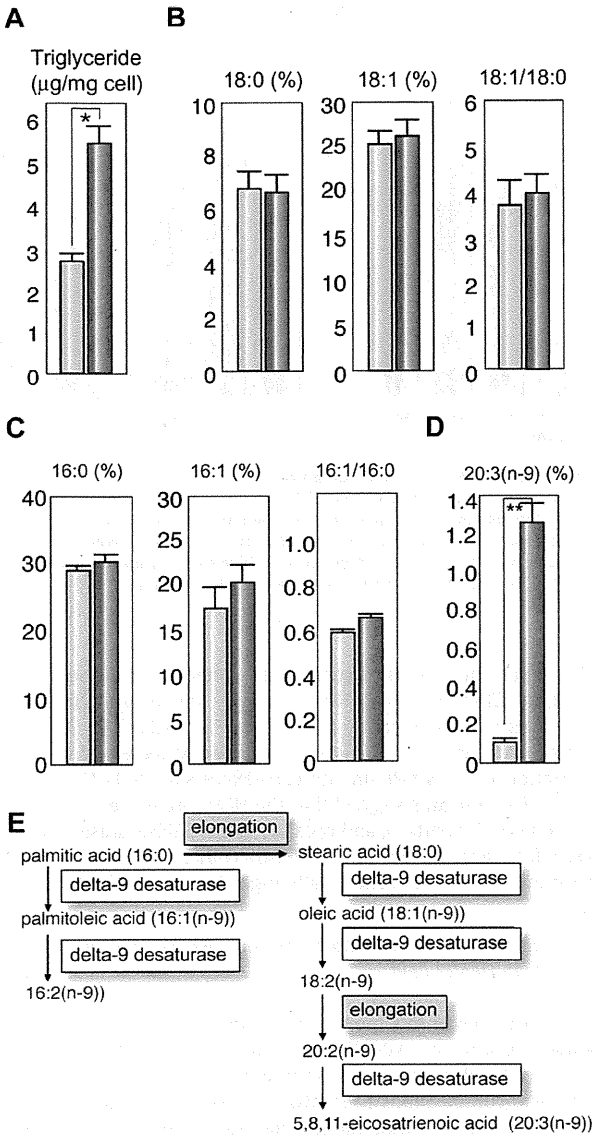

Fig. 1. Effect of the core protein on fatty acid composition in HepG2 cells. The fatty acid compositions of the total cell lipids were analyzed and the ratios of 18:1/18:0 and 16:1/16:0 in the core-expressing and control HepG2 cells were calculated. (A) Concentrations of triglycerides. (B) Percentages of stearic acid (18:0) and oleic acid (18:1(n-9)), and the 18:1/18:0 ratio. (C) Percentages of palmitic acid (16:0) and palmitoleic acid (16:1(n-9)), and the 16:1/16:0 ratio. (D) Percentage of eicosatrienoic acid (20:3(n-9). (E) Schematic display of synthetic pathway of n-9 fatty acids. Light blue bars indicate control cells and dark blue bars indicate core-expressing cells. Values represent the mean ± SE, $n = 5$ in each group. $^{*}p < 0.05$, $^{**}p < 0.01$.

Previously, we reported that the concentration of oleic acid (18:1(n-9)) was increased compared with that of stearic acid (18:0) in liver tissues of chronic hepatitis C patients as well as in those of mice transgenic for the HCV core gene [8]. Such a change may lead to increased membrane fluidity, owing to the lower melting temperature of monounsaturated fatty acids, resulting in incremental metabolism and proliferation of hepatocytes [20–22]. On the other hand, polyunsaturated fatty acids (PUFAs), such as eicosapentaenoic acid (20:5(n-3)) and arachidonic acid (20:4(n-6)), are known to activate the nuclear transcription of peroxisome proliferator-activated receptors (PPAR) and suppress the sterol regulatory element binding protein (SREBP)-1. While PPARγ induces delta-9 desaturase (stearoyl-CoA desaturase) gene expression, PUFAs suppresses delta-9 desaturase activity [23]. In the current study, we determined fatty acid desaturase activities by analyzing the fatty acid compositions in HepG2 cells expressing HCV core protein by chromatography. In addition, we determined whether exogenous PUFAs restore HCV-associated changes in fatty acid metabolism.

Materials and methods

Reagents

Eicosapentaenoic acid (EPA), arachidonic acid (AA), and eicosatetraynoic acid (ETYA) were purchased from Sigma Chemical (St. Louis, MO). Other chemicals were of analytical grade and purchased from Wako Chemicals (Tokyo, Japan).

Cell culture

This study was performed using HepG2 cell lines expressing the HCV core protein under the control of the CAG promoter (Hep39J, Hep396 and Hep397), or a control HepG2 line (Hepswx) carrying an empty vector, which were described previously [24], and control bulk HepG2 cells. They were maintained in Dulbecco's modified Eagle's medium (DMEM), supplemented with 10% fetal bovine serum (Invitrogen), 1 mg/ml G418, 100 U/ml penicillin, and 100 μg/ml streptomycin in a humidified atmosphere at 37 °C in 5% CO_2. Fatty acids were dissolved in DMEM containing defatted bovine serum albumin. The ratio of fatty acids to albumin (mole/mole) was 0.7. The cells were exposed to fatty acid–albumin complexes at various concentrations for 48 h. All the experiments were repeated at least five times.

Lipid extraction, measurement of triglyceride content, and analysis of fatty acid composition

Total cell lipids were extracted by Foch's method. The cells were washed twice with phosphate-buffered saline and collected by centrifugation. The cell pellets were homogenized with 10 vole of chloroform: methanol solution (2:1), and the mixture was shaken for 5 min. The lower phase was then washed with 4 vole of saline, dried on anhydrous sodium sulfate, and evaporated to complete dryness. For the analysis of fatty acid composition, the residue was methanolysed by the modified Morrison and Smith method with boron trifluoride as a catalyst [25]. Fatty acid methyl esters were analyzed using a Shimadzu GC-7A gas chromatograph (Shimadzu Corp., Kyoto, Japan).

Measurement of the ketone body ratio and lactate/pyruvate

The cells were cultured to confluence on 3.5 cm dishes, and the medium was replaced with 700 μl of fresh one. After 24 h of incubation, the levels of acetoacetate and β-hydroxybutyrate in the medium were measured by monitoring the production or consumption of nicotinamide adenine dinucleotide (NADH) with Ketorex kit (Sanwa Chemical, Nagoya, Japan) [26]. The ketone body ratio (KBR) was calculated as the acetoacetate/β-hydroxybutyrate ratio. The lactate and pyruvate levels in the medium were measured at random times by the lactate oxidase method and pyruvate oxidase method, respectively.

Effect of pyruvate on lipid metabolism

In some experiments, pyruvate (Wako Chemicals) was added to culture medium at a final concentration of 0, 1, 5, or 10 mM. After 48 h of incubation at 37 °C, the cells were harvested and subjected to fatty acid composition analysis or real-time PCR analysis.

Research Article

Real-time PCR

RNA was prepared from cultured cells using TRIzol LS (Invitrogen, Carlsbad, CA). The fluorescent signal was measured using ABI prism 7000 (Applied Biosystems, Tokyo, Japan). The genes encoding mouse sterol regulatory element-binding proteins (SREBP)-1a, SREBP-1c, delta-9 desaturase, and hypoxanthine phosphoribosyltransferase were amplified with the primer pairs CACAGCGGTTTTGAACGAC and CTGGCTCCTCTTTGATCCCA, ACGGAGCCATGGATTGCACATTTG and TACATCTT TAAAGCAGCGGGTGCCGATGGT, TTCCCTCCTGCAAGCTCTAC and CGCAAGAAGG TGCTAACGAAC, and CCAGCAAGCTTGCAACCTTAACCA and GTAATGATCAGTCAAC GGGGGAC, respectively.

Statistical analysis

Data are presented as the mean ± SE. The data were analyzed by Mann–Whitney *U* test. Differences were considered statistically significant when $p < 0.05$.

Results

Triglyceride content in HepG2 cells expressing HCV core protein

To validate the relationship between the lipid accumulation and the core protein, we first determined the triglyceride contents in core-protein-expressing HepG2 clones (core-expressing cells), Hep39J, Hep396, Hep397, and control HepG2 cells. Core-expressing Hep396 cells contained significantly larger amounts of triglyceride than the control cells (Fig. 1A, $p < 0.01$), which are consistent with the results of previous studies on culture cells and transgenic mice [6,7,27]. Similar results were obtained with the other core-expressing cell lines.

Fatty acid compositions of total cell lipids

Analysis on the fatty acid compositions of total lipids revealed that the concentration of oleic acid (18:1(n-9)) and the ratio of oleic acid/stearic acid (18:1/18:0) in the core-expressing cells are similar to those in the control cells (Fig. 1B). The ratio of palmitoleic acid (16:1(n-9))/palmitic acid (16:1/16:0) was higher in the core-expressing cells than that in the control cells, but the difference was not significant (Fig. 1C). This rather dissociates from the results obtained in HCV core gene transgenic mice, in which the 18:1/18:0 ratio was significantly higher than that in control mice, thereby suggesting an increased delta-9 desaturase activity as a consequence of the HCV core protein expression [8]. However, it should be noted that the concentration of 5,8,11-eicosatrienoic acid (20:3(n-9)), a downstream product of n-9 fatty acid desaturation, was approximately13 times higher in the core-expressing cells than that in the control cells (Fig. 1D and E, $p < 0.01$). This is due to the fact that the activity of the delta-6 desaturase, an enzyme downstream of delta-9 desaturase, is also high in HepG2 cells, resulting in the relatively lower concentration of 18:1 in the core-expressing cells despite the high delta-9 desaturase activity. Actually, the delta-6 desaturase activity has been shown to be inherently high in HepG2 cells [28,29].

To verify this possibility, we administered ETYA, which inhibits delta-6 desaturase activity, to the cell cultures. Because similar results were obtained with the other core-expressing HepG2 cell lines, subsequent experiments were carried out using the Hep396 cell line. The addition caused significant increases in both 18:1/18:0 and 16:1/16:0 ratios in the core-expressing cells but not in the control cells (Fig. 2A 0 vs. 10 μg/ml and 0 vs. 50 μg/ml; $p < 0.05$, respectively). When compared between the

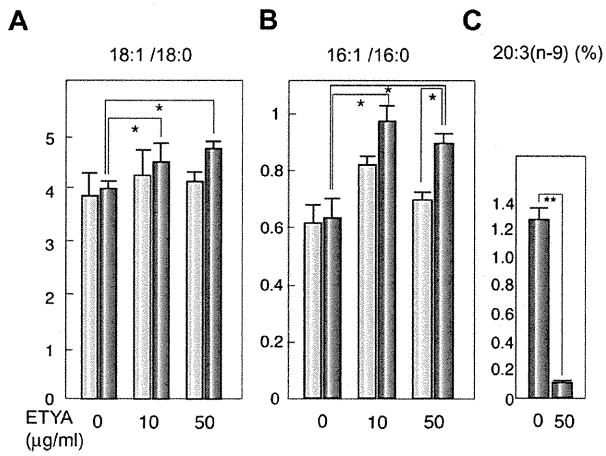

Fig. 2. Effect of ETYA on delta-9 desaturase index. HepG2 cells with or without the core protein were incubated with ETYA for 48 h. The fatty acid compositions of the total cell lipids were analyzed, and the ratios of 18:1/18:0 (A) and 16:1/16:0 (B), and the percentage of eicosatrienoic acid (20:3(n-9) (C) were computed. Light blue bars indicate control cells and dark blue bars indicate core-expressing cells. $N = 5$ in each group. *$p < 0.05$. ETYA, eicosatetraynoic acid.

core-expressing cells and control cells after the treatment with 50 μg/ml ETYA, the 18:1/18:0 ratio was higher and the 16:1/16:0 ratio was significantly higher (Fig. 2B, $p < 0.05$) in the core-expressing cells. ETYA (50 μg/ml) significantly decreased the concentration of 20:3(n-9) in the core-expressing cells (Fig. 2C, $p < 0.01$). These results suggest that the HCV core protein enhances the activities of delta-9, and possibly, delta-5 desaturases, modulating fatty acid metabolism in HepG2 cells, in which the delta-6 desaturase activity is intrinsically high (Fig. 1E) [28,29].

PUFAs modify fatty acid compositions and decrease triglyceride contents in HepG2 Cells

PUFAs are known to suppress the activities of both delta-9 and delta-6 desaturases. We, therefore, added PUFA, EPA, or AA, to the culture cell medium to examine the effect of PUFAs on the fatty acid compositions in HepG2 cells expressing the core protein. EPA and AA individually decreased the 18:1/18:0 and 16:1/16:0 ratios in a similar extent in both the core-expressing cells and the control cells (Fig. 3, $p < 0.05$). EPA and AA also significantly decreased the concentration of 20:3(n-9) in the core-expressing cells in a dose-dependent manner (Fig. 4, $p < 0.05$). In addition, EPA and AA individually decreased the triglyceride concentration in cells, in particular, in the core-expressing cells (Fig. 5, in core-expressing cells, $p < 0.01$; in control cells, $p < 0.05$, respectively).

Ketone body ratio and lactate/pyruvate ratio

Although the mechanism by which the HCV core protein enhances fatty acid desaturation is yet unclear, one possibility is the creation of an overreduced state in the core-expressing cells. The overreduced state or the accumulation of NADH in cells is known to accelerate the activities of fatty acid desaturases [30,31]. Such a condition may originate from the dysfunction of the mitochondrial electron transfer system (ETS), which has been

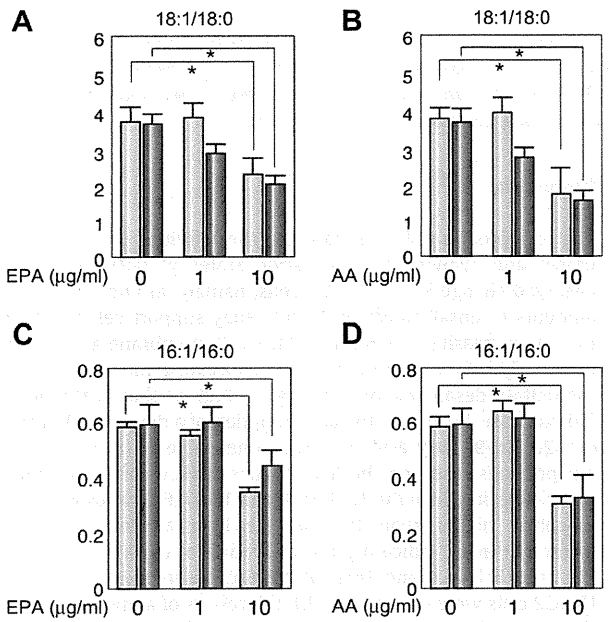

Fig. 3. Effect of EPA and AA on delta-9 desaturase index. HepG2 cells with or without the core protein were incubated with EPA (A and C) or AA (B and D) for 48 h. The fatty acid compositions of the total cell lipids were analyzed and the ratios of 18:1/18:0 (A and B) and 16:1/16:0 (C and D) were computed. Light blue bars indicate control cells and dark blue bars indicate core-expressing cells. $N = 5$ in each group. $^{*}p < 0.05$. EPA, eicosapentaenoic acid; AA, arachidonic acid.

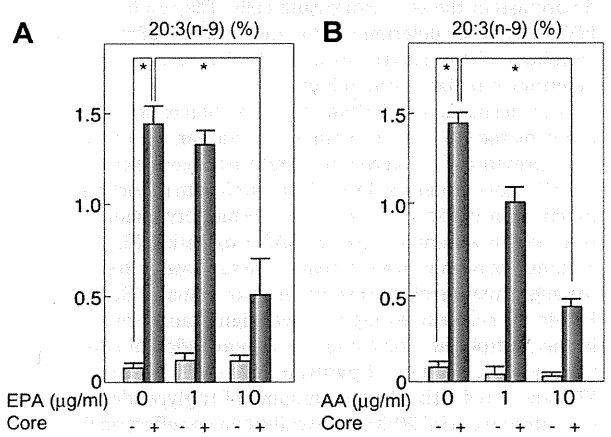

Fig. 4. Effect of EPA and AA on the concentration of 20:3(n-9). HepG2 cells with or without the core protein were incubated with EPA (A) or AA (B) for 48 h. The fatty acid compositions of the total cell lipids were analyzed and the percentages of the C20:3(n-9) fraction were measured. Light blue bars indicate control cells and dark blue bars indicate core-expressing cells. $N = 5$ in each group. $^{*}p < 0.05$.

suggested to be associated with HCV infection by the action of the HCV core protein [32–35]. Then, we explored the possibility that an increase in the NADH level, which is caused by the mitochondrial ETS dysfunction, induces the activation of fatty acid desaturases. Because fatty acid synthesis or fatty acid desaturation is accompanied by the oxidation of NAD(P)H, we measured the ketone body ratio (KBR) in the culture medium to estimate the redox state in the HepG2 cells expressing the core protein.

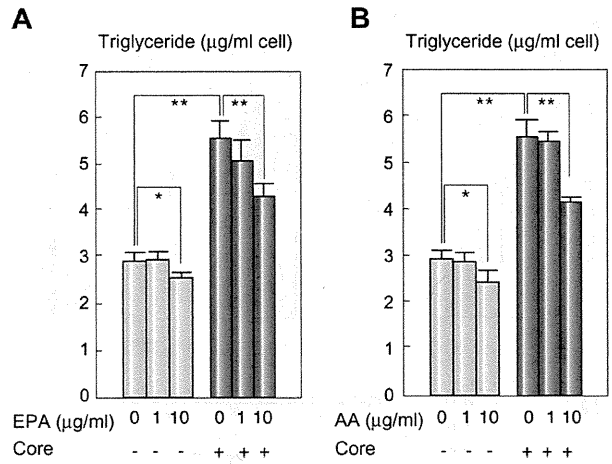

Fig. 5. Effect of EPA and AA on triglyceride content. HepG2 cells with or without the core protein were incubated with EPA (A) or AA (B) for 48 h. The triglyceride volume of the total cell lipids was measured and the triglyceride contents in the cells were calculated. Light blue bars indicate control cells and dark blue bars indicate core-expressing cells. $N = 5$ in each group. $^{*}p < 0.05$, $^{**}p < 0.01$.

The KBR, which is in equilibrium with the intramitochondrial $NAD^+/NADH$ [26,36], in the culture medium of the core-expressing cells, was significantly lower than that of control cells (Fig. 6A, $p < 0.01$). The ratio of lactate to pyruvate (lactate/pyruvate), which is proportional to the cytosolic $NADH/NAD^+$ [26], in the culture medium of the core-expressing cells was significantly higher than that of control cells (Fig. 6B, $p < 0.05$). These results, the higher $NADH/NAD^+$ ratio in both determinations, indicate that NADH accumulates in the core-expressing HepG2 cells, resulting in the overreduced state, as a consequence of the core protein expression. The amounts of total ketone bodies were significantly higher in the core-expressing cells than that in the control cells (Fig. 6C).

Effects of pyruvate on lipid metabolism in core-expressing cells

The addition of pyruvate into this constitutive core protein expression system, in which the pyruvate metabolism is in equilibrium, is expected to cause a reduction in the NADH level along with increases in the levels of lactate and NAD^+, because pyruvate tends to be converted to lactate by the action of lactate dehydrogenase (LDH) under the condition of high $NADH/NAD^+$ ratio [26,36]. Actually, the addition of pyruvate into the culture medium at various concentrations increased the KBR and reduced the amount of 5,8,11-eicosatrienoic acid (20:3 (n-9)) (Fig. 6D, $p < 0.05$ at 10 mM pyruvate), while it had no effect on the control cells. It also caused a reduction in the amount of triglyceride in the core-expressing cells but not in the control cells (Fig. 6E). This finding strongly supports the notion that NADH accumulation is, at least, one of the causes of the activation of fatty acid desaturases in this HCV model. The mRNA levels of anti-oxidant genes significantly decreased after the incubation with pyruvate at 10 mM (catalase, 1.27 ± 0.06 vs. 0.91 ± 0.05; glutathione synthetase 1.39 ± 0.04 vs. 1.01 ± 0.06; glutathione peroxidase 1.48 ± 0.03 vs. 1.23 ± 0.07, pyruvate (−) vs. pyruvate (+), $p < 0.05$, respectively), suggesting that pyruvate reduced the levels of oxidative stress in the core-expressing HepG2 cells.

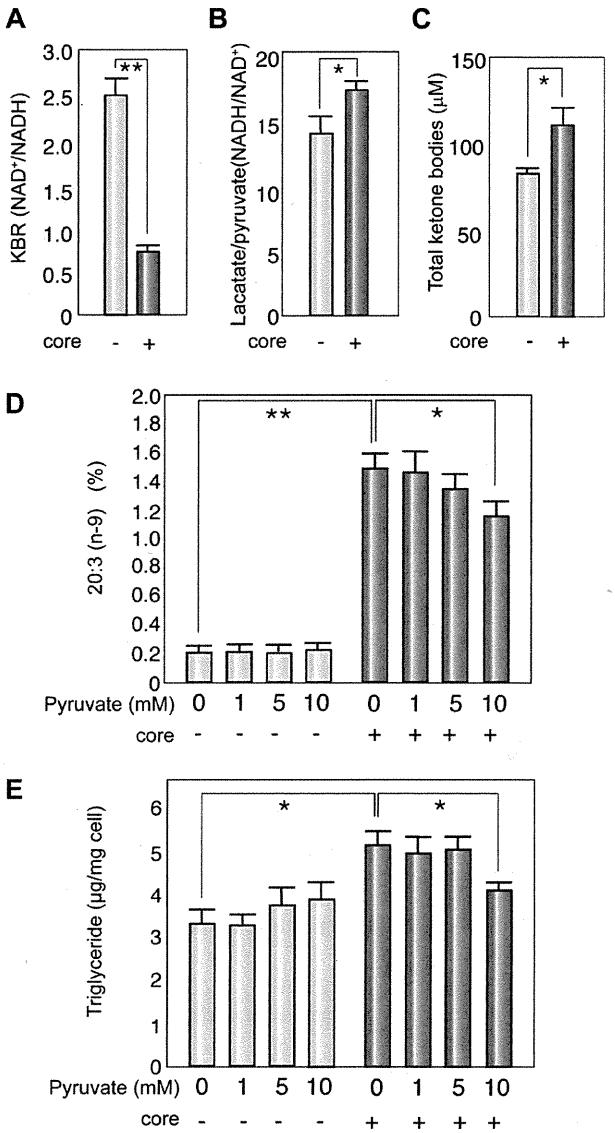

Fig. 6. NADH accumulation and effect of pyruvate in core-expressing cells. HepG2 cells with or without the core protein were subjected to the determination of ketone body ratio (A) and lactate/pyruvate ratio (B) for the precise estimation of NAD^+/NADH and NADH/NAD^+. (C) Total ketone bodies. (D) The percentages of the C20:3(n-9) fraction were measured after incubation with pyruvate at various concentrations. (E) The total amount of triglyceride was measured after incubation with pyruvate at various concentrations. Light blue bars indicate control cells and dark blue bars indicate core-expressing cells. $N = 5$ in each group. $^*p < 0.05$, $^{**}p < 0.01$.

Expression of SREBP-1 and desaturase genes in core-expressing cells

We previously showed that the core protein activates the expression of the SREBP-1c gene, which regulates the production of triglyceride [37] in the liver. We, therefore, examined the mRNA levels of genes associated with lipid metabolism in the current system. As shown in Fig. 7, the mRNA levels of SREBP-1c and delta-9 (stearoyl CoA) desaturase genes, but not that of the SREBP-1a gene, were significantly higher in the core-expressing cells than that in the control cells. Of note, the mRNA levels of the former two genes significantly decreased after the incubation with AA. The treatment with pyruvate also reduced the mRNA levels of the two genes, but the difference was not statistically significant compared with the control.

Discussion

The core protein of HCV modulated the activities of delta desaturases and changed the saturation states of fatty acids. The observed change in the HepG2 cells, namely, an increase in the amounts of unsaturated fatty acids, may support cell proliferation, by increasing the fluidity of the cell membrane as reported previously [20]. In the HepG2 cells expressing the core protein, the delta-6 desaturase activity was as high as that of the delta-9 desaturase, leading to the accumulation of a downstream product, 20:3(n-9) fatty acid. This was, unexpectedly, in contrast to our previous result on the liver tissues of HCV core gene transgenic mice, in which the 18:1/18:0 and 16:1/16:0 ratios were significantly higher than that in the liver tissues of normal littermate mice, indicating the activation of delta-9 desaturase [8]. The 16:1/16:0 and 18:1/18:0 ratios observed in the control HepG2 cells were consistent with the results of a previous study: the delta-6 desaturase activity is inherently higher in HepG2 cells than in normal mouse hepatocytes [28,29]. This may explain the difference in the effect of the core protein on lipid metabolism in these two systems, namely, HepG2 cells and mouse liver tissues. The significant increase in the delta-9 desaturase index and high concentration of 20:3(n-9) by the administration of ETYA, a delta-6 desaturase inhibitor, indicate the activation of delta-9 desaturase in the core-expressing cells. The results of real-time PCR analysis for determining the mRNA levels of these enzymes corroborated the current estimation of desaturase activities as determined by fatty acid analysis.

The mechanism underlying the activation of fatty acid desaturation by the HCV core protein is still unclear, but one possibility is the presence of an overreduced state in the core-expressing cells. The HCV core protein is closely associated with mitochondrial dysfunction, in particular, that of the respiratory chain complexes, resulting in an impairment of NADH oxidation [32–35]. NADH accumulation leads to an increase in desaturase activities through the augmentation of microsomal electron transfer [38]. In fact, the KBR in the core-expressing cells was significantly lower than that in the control cells, indicating the accumulation of NADH within the cells. The addition of pyruvate resulted in an increase in the KBR and a reduction in the amounts of triglyceride and 5,8,11-eicosatrienoic acid (20:3 (n-9)) while it had no effect on the control cells, strongly supporting the notion that NADH accumulation induced by the core protein is, at least, one of the causes of the activation of fatty acid desaturases in this HCV model.

Another possible mechanism underlying the accelerated desaturation is the activation of SREBP-1c, which controls the expression of delta-9 desaturase. In fact, the level of SREBP-1c mRNA was higher in the core-expressing cells than that in the control cells as reported previously [37]. The relief of NADH accumulation by pyruvate administration resulted in the reduced accumulation of triglyceride and unsaturated fatty acids, which was accompanied by the reduction in SREBP-1c and delta-9 desaturase gene expression levels. The intracellular accumulation of NADH might be involved in the activation of the SREBP-1c gene expression by the core protein. Thus, NADH accumulation, which

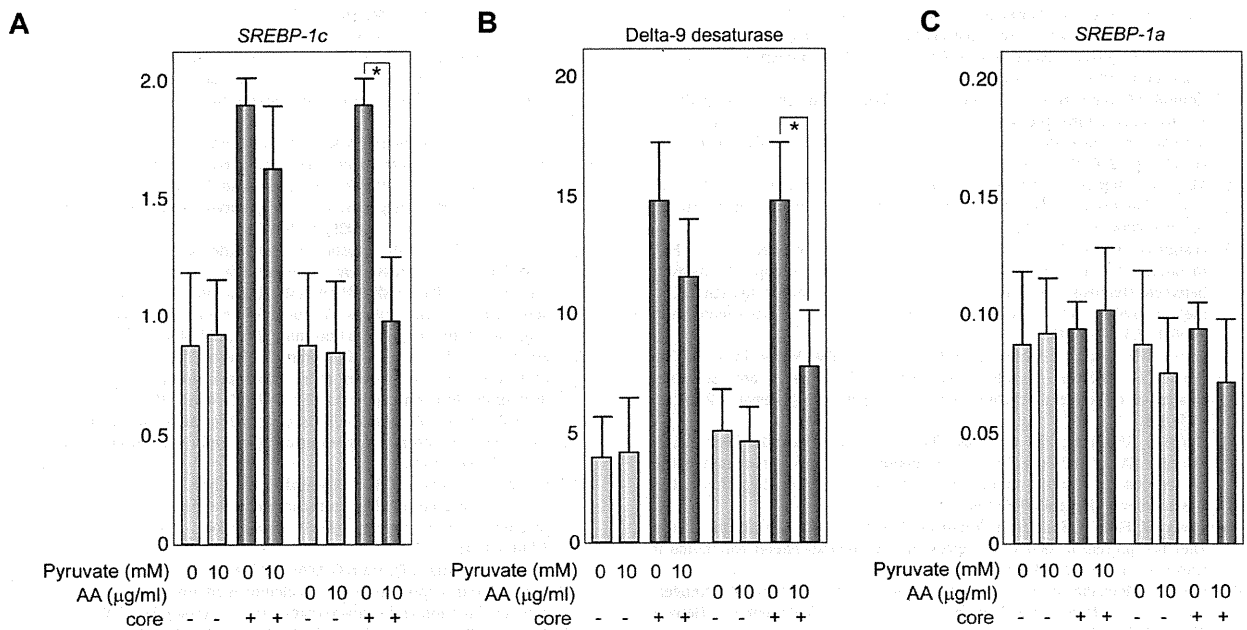

Fig. 7. Effect of pyruvate and AA on mRNA levels of lipid-associated genes. The mRNA levels of *SREBP-1c* (A), delta-9 desaturase (B) and *SREBP-1a* (C) genes were determined by real-time PCR analysis. The transcription of the genes was normalized with that of hypoxanthine phosphoribosyltransferase, and the values are expressed as relative activities. Light blue bars indicate control cells and dark blue bars indicate core-expressing cells. $N = 5$ in each group. $^*p < 0.05$. SREBP, sterol regulatory element binding protein.

is induced by the core protein through the impairment of the mitochondrial complex function [35], may be a key event that leads to the SREBP-1c activation, the desaturase activation, and the development of steatosis associated with HCV infection.

EPA and AA (PUFAs), which are known to suppress desaturase activities, lowered the 18:1/18:0 and 16:1/16:0 ratios and decreased the concentration of 20:3(n-9) concomitantly with that of triglyceride, regardless of the presence of the core protein, probably through SREBP-1c suppression (Fig. 7) [39]. On the other hand, the administration of EPA or AA did not affect the KBR in the core-expressing or control cells (data not shown), limiting the PUFAs ability to counteract the effect of the core protein. This is in contrast to the fact that the addition of pyruvate caused an increase in the KBR and a reduction in the amounts of triglyceride and 5,8,11-eicosatrienoic acid (20:3 (n-9)), while it had no effect on the control cells.

Fatty acid desaturation is closely associated with increased membrane fluidity [20], leading to augmented cell metabolism and higher cell division rates [21,22]. Although the relationship between carcinogenesis and lipid metabolism altered by the HCV core protein remains to be further clarified, alterations in lipid metabolism, in particular, in the desaturation of fatty acids, are closely associated with HCV infection, and PUFAs could prevent the pathogenesis of HCV-associated disorders involving lipid metabolism.

Conflict of interest

The authors who have taken part in this study declared that they do not have anything to disclose regarding funding or conflict of interest with respect to this manuscript.

Acknowledgments

This work was supported in part by Grant-in-Aid for Scientific Research on Priority Area from the Ministry of Education, Science, Sports, and Culture of Japan; Health Sciences Research Grants of The Ministry of Health, Labour, and Welfare (Research on Hepatitis); and a grant from The Sankyo Foundation of Life Science.

References

[1] Saito I, Miyamura T, Ohbayashi A, Harada H, Katayama T, Kikuchi S, et al. Hepatitis C virus infection is associated with the development of hepatocellular carcinoma. Proc Natl Acad Sci USA 1990;87:6547–6549.
[2] Schemer PJ, Ashrafzadeh P, Sherlock S, Brown D, Dusheiko GM. The pathology of chronic hepatitis C. Hepatology 1992;15:567–571.
[3] Bach N, Thung SN, Schaffner F. The histological features of chronic hepatitis C and autoimmune chronic hepatitis: a comparative analysis. Hepatology 1992;15:572–577.
[4] Fujie H, Yotsuyanagi H, Moriya K, Shintani Y, Tsutsumi T, Takayama T, et al. Steatosis and intrahepatic hepatitis C virus in chronic hepatitis. J Med Virol 1999;59:141–145.
[5] Moradpour D, Englert C, Wakita T, Wands JR. Characterization of cell lines allowing tightly regulated expression of hepatitis C virus core protein. Virology 1996;222:51–63.
[6] Barba G, Harper F, Harada T, Kohara M, Goulinet S, Matsuura Y, et al. Hepatitis C virus core protein shows a cytoplasmic localization and associates to cellular lipid storage droplets. Proc Natl Acad Sci USA 1997;94:1200–1205.
[7] Moriya K, Yotsuyanagi H, Shintani Y, Fujie H, Ishibashi K, Matsuura Y, et al. Hepatitis C virus core protein induces hepatic steatosis in transgenic mice. J Gen Virol 1997;78:1527–1531.
[8] Moriya K, Todoroki T, Tsutsumi T, Fujie H, Shintani Y, Miyoshi H, et al. Increase in the concentration of carbon 18 monosaturated fatty acids in the liver with hepatitis C: analysis in transgenic mice and humans. Biophys Biochem Res Commun 2001;281:1207–1212.
[9] Lerat H, Honda M, Beard MR, Loesch K, Sun J, Yang Y, et al. Steatosis and liver cancer in transgenic mice expressing the structural and nonstructural proteins of hepatitis C virus. Gastroenterology 2002;122:352–365.

Research Article

[10] Naas T, Ghorbani M, Alvarez-Maya I, Lapner M, Kothary R, De Repentigny Y, et al. Characterization of liver histopathology in a transgenic mouse model expressing genotype 1a hepatitis C virus core and envelope proteins 1 and 2. J Gen Virol 2005;86:2185–2196.

[11] Adinolfi LE, Gambardella M, Andreana A, Tripodi MF, Utili R, Ruggiero G. Steatosis accelerates the progression of liver damage of chronic hepatitis C patients and correlates with specific HCV genotype and visceral obesity. Hepatology 2001;33:1358–1364.

[12] Massard J, Ratziu V, Thabut D, Moussalli J, Lebray P, Benhamou Y, et al. Natural history and predictors of disease severity in chronic hepatitis C. J Hepatol 2006;44:S19–S24.

[13] Leandro G, Mangia A, Hui J, Fabris P, Rubbia-Brandt L, Colloredo G, et al. HCV meta-analysis (on) individual patients' data study group. Relationship between steatosis, inflammation, and fibrosis in chronic hepatitis C: a meta-analysis of individual patient data. Gastroenterology 2006;130:1636–1642.

[14] Patton HM, Patel K, Behling C, Bylund D, Blatt LM, Vallee M, et al. The impact of steatosis on disease progression and early and sustained treatment response in chronic hepatitis C patients. J Hepatol 2004;40: 484–490.

[15] Harrison SA, Brunt EM, Qazi RA, Oliver DA, Neuschwander-Tetri BA, Di Bisceglie AM, et al. Effect of significant histologic steatosis or steatohepatitis on response to antiviral therapy in patients with chronic hepatitis C. Clin Gastroenterol Hepatol 2005;3:604–609.

[16] Moriya K, Fujie H, Shintani Y, Yotsuyanagi H, Tsutsumi T, Ishibashi K, et al. The core protein of hepatitis C virus induces hepatocellular carcinoma in transgenic mice. Nat Med 1998;4:1065–1067.

[17] Koike K. Molecular basis of hepatitis C virus-associated hepatocarcinogenesis: lessons from animal model studies. Clin Gastroenterol Hepatol 2005;3:S132–S135.

[18] Shi ST, Lee KJ, Aizaki H, Hwang SB, Lai MM. Hepatitis C virus RNA replication occurs on a detergent-resistant membrane that cofractionates with caveolin-2. J Virol 2003;77:4160–4168.

[19] Miyanari Y, Atsuzawa K, Usuda N, Watashi K, Hishiki T, Zayas M, et al. The lipid droplet is an important organelle for hepatitis C virus production. Nat Cell Biol 2007;9:1089–1097.

[20] Stubbs CD, Smith AD. The modification of mammalian membrane polyunsaturated fatty acid composition in relation to membrane fluidity and function. Biochim Biophys Acta 1984;779:89–137.

[21] Li J, Ding SF, Habib NA, Fermor BF, Wood CB, Gilmour RS. Partial characterization of a cDNA for human stearoyl-CoA desaturase and changes in its mRNA expression in some normal and malignant tissues. Int J Cancer 1994;57:348–352.

[22] Vinciguerra M, Carrozzino F, Peyrou M, Carlone S, Montesano R, Benelli R, et al. Unsaturated fatty acids promote hepatoma proliferation and progression through downregulation of the tumor suppressor PTEN. J Hepatol 2009;50:1132–1141.

[23] Ntambi JM. Regulation of stearoyl-CoA desaturase by polyunsaturated fatty acids and cholesterol. J Lipid Res 1999;40:1549–1558.

[24] Ruggieri A, Murdolo M, Harada T, Miyamura T, Rapicetta M. Cell cycle perturbation in a human hepatoblastoma cell line constitutively expressing hepatitis C virus core protein. Arch Virol 2004;149:61–74.

[25] Morrison WR, Smith LM. Preparation of fatty acid methyl esters and dimethylacetals from lipids with boron fluoride–methanol. J Lipid Res 1964;5:600–608.

[26] Williamson DH, Mellanby J, Krebs HA. Enzymic determination of D(-)-beta-hydroxybutyric acid and acetoacetic acid in blood. Biochem J 1962;82:90–96.

[27] Abid K, Pazienza V, Gottardi A, Rubbia-Brandt L, Conne B, Pugnale P, et al. An in vitro model of hepatitis C virus genotype 3a-associated triglycerides accumulation. J Hepatol 2005;42:744–751.

[28] Portolesi R, Powell BC, Gibson RA. Delta6 desaturase mRNA abundance in HepG2 cells is suppressed by unsaturated fatty acids. Lipids 2008;43:91–95.

[29] Choi Y, Park Y, Pariza MW, Ntambi JM. Regulation of stearoyl-CoA desaturase activity by the trans-10, cis-12 isomer of conjugated linoleic acid in HepG2 cells. Biochem Biophys Res Commun 2001;284:689–693.

[30] Strittmatter P, Spatz L, Corcoran D, Rogers MJ, Setlow B, Redline R. Purification and properties of rat liver microsomal stearyl coenzyme a desaturase. Proc Natl Acad Sci USA 1974;71:4565–4569.

[31] Joshi VC, Wilson AC, Wakil SJ. Assay for the terminal enzyme of the stearoyl coenzyme A desaturase system using chick embryo liver microsomes. J Lipid Res 1977;18:32–36.

[32] Korenaga M, Wang T, Li Y, Showalter LA, Chan T, Sun J, et al. Hepatitis C virus core protein inhibits mitochondrial electron transport and increases reactive oxygen species (ROS) production. J Biol Chem 2005;280: 37481–37488.

[33] Piccoli C, Scrima R, Quarato G, D'Aprile A, Ripoli M, Lecce L, et al. Hepatitis C virus protein expression causes calcium-mediated mitochondrial bioenergetic dysfunction and nitro-oxidative stress. Hepatology 2007;46:58–65.

[34] Tsutsumi T, Matsuda M, Aizaki H, Moriya K, Miyoshi H, Fujie H, et al. Proteomics analysis of mitochondrial proteins reveals overexpression of a mitochondrial protein chaperone, prohibitin, in cells expressing hepatitis C virus core protein. Hepatology 2009;50:378–386.

[35] Moriya K, Miyoshi H, Tsutsumi T, Shinzawa S, Fujie H, Shintani Y, et al. Tacrolimus ameliorates metabolic disturbance and oxidative stress caused by hepatitis C virus core protein: Analysis using mouse model and cultured cells. Am J Pathol 2009;175:1515–1524.

[36] Williamson DH, Lund P, Krebs HA. The redox state of free nicotinamide-adenine dinucleotide in the cytoplasm and mitochondria of rat liver. Biochem J 1967;103:514–527.

[37] Moriishi K, Mochizuki R, Moriya K, Miyamoto H, Mori Y, Abe T, et al. Critical role of PA28gamma in hepatitis C virus-associated steatogenesis and hepatocarcinogenesis. Proc Natl Acad Sci USA 2007;104:1661–1666.

[38] Jansson I, Schenkman JB. Studies on three microsomal electron transfer enzyme systems. Specificity of electron flow pathways. Arch Biochem Biophys 1977;178:89–107.

[39] Sekiya M, Yahagi N, Matsuzaka T, Najima Y, Nakakuki M, Nagai R, et al. Polyunsaturated fatty acids ameliorate hepatic steatosis in obese mice by SREBP-1 suppression. Hepatology 2003;38:1529–1539.

Clinica Chimica Acta 412 (2011) 1201–1206

Contents lists available at ScienceDirect

Clinica Chimica Acta

journal homepage: www.elsevier.com/locate/clinchim

Autotaxin as a novel serum marker of liver fibrosis

Hayato Nakagawa [a,b], Hitoshi Ikeda [a,b,*], Kazuhiro Nakamura [a], Ryunosuke Ohkawa [a], Ryota Masuzaki [b], Ryosuke Tateishi [b], Haruhiko Yoshida [b], Naoko Watanabe [a,b], Kazuaki Tejima [c], Yukio Kume [a], Tomomi Iwai [a], Atsushi Suzuki [a], Tomoaki Tomiya [b], Yukiko Inoue [b], Takako Nishikawa [b], Natsuko Ohtomo [b], Yasushi Tanoue [b], Masao Omata [d], Koji Igarashi [e], Junken Aoki [f], Kazuhiko Koike [b], Yutaka Yatomi [a]

[a] Department of Clinical Laboratory Medicine, Graduate School of Medicine, The University of Tokyo, Tokyo, Japan
[b] Department of Gastroenterology, Graduate School of Medicine, The University of Tokyo, Tokyo, Japan
[c] Department of Gastroenterology, Toshiba General Hospital, Tokyo, Japan
[d] Yamanashi Prefectural Hospital Organization, Yamanashi, Japan
[e] Bioscience Division, Reagent Development Department, AIA Research Group, TOSOH Corporation, Kanagawa, Japan
[f] Department of Molecular and Cellular Biochemistry, Graduate School of Pharmaceutical Sciences, Tohoku University, Miyagi, Japan

ARTICLE INFO

Article history:
Received 7 February 2011
Received in revised form 3 March 2011
Accepted 10 March 2011
Available online 17 March 2011

Keywords:
Autotaxin
Lysophospholipase D
Hyaluronic acid
Liver stiffness
Liver fibrosis
Lysophosphatidic acid

ABSTRACT

Background: The clinical significance of autotaxin (ATX), a key enzyme for the production of the bioactive lysophospholipid lysophosphatidic acid remains unknown. Serum ATX enzymatic activity reportedly increases in parallel with liver fibrosis and exhibits a gender difference.
Methods: Serum ATX antigen level, measured easier than the activity, was evaluated as a marker of liver fibrosis in 2 cohorts of chronic liver disease caused by hepatitis C virus.
Results: In the first cohort, serum ATX level correlated significantly with liver fibrosis stage and was the best parameter for prediction of cirrhosis with an area under the receiver operating characteristic curve (AUROC) of 0.756 in male and 0.760 in female, when compared with serum hyaluronic acid and aminotransferase-to-platelet ratio index, an established marker of liver fibrosis. In another cohort, serum ATX level correlated significantly with liver stiffness, a novel reliable marker of liver fibrosis, being the second-best parameter in male (AUROC, 0.799) and in female (AUROC, 0.876) for prediction of significant fibrosis, and the best parameter in male (AUROC, 0.863) and the third-best parameter in female (AUROC, 0.872) for prediction of cirrhosis, both of which were judged by liver stiffness.
Conclusions: Serum ATX level may be a novel marker of liver fibrosis.

1. Introduction

The bioactive lysophospholipid lysophosphatidic acid (1- or 2-acyl-lysophosphatidic acid; LPA) elicits a variety of biological responses, such as neurogenesis, angiogenesis, smooth-muscle contraction, platelet aggregation, and wound healing [1,2]. LPA has also been shown to contribute to cancer progression and metastasis [3,4]. From a clinical viewpoint, LPA is reportedly increased in the plasma of ovarian cancer patients, compared with healthy control subjects [5]. Furthermore, LPA is reportedly present in minimally modified LDL and within the intima of atherosclerotic lesions, where it may play a role in the early phase of atherosclerosis [6]. Thus, the information on how and where LPA is produced in the body fluids, especially the plasma and serum, is very important. This, however, had long remained unknown until recently. LPA production in the serum reportedly involves several phospholipases, including phosphatidylserine-specific phospholipase A1, secretory phospholipase A2 group IIA, lecithin-cholesterol acyltransferase, and lysophospholipase D (lysoPLD) [7]. In particular, lysoPLD is the most important enzyme for the production of serum LPA. This lipase hydrolyzes lysophospholipids, mainly lysophosphatidylcholine, to produce LPA. Two different groups succeeded in cloning lysoPLD and found that this enzyme is identical to the soluble form of autotaxin (ATX) [8,9]; ATX was originally isolated from the conditioned medium of A2058 human melanoma cells as a potent cell motility-stimulating factor [10]. The enhanced expression of ATX has been reported in various malignant tumor tissues, such as non-small cell lung cancer [11]. The (patho)physiological functions of ATX are now thought to be explained by its ability to produce LPA [7–9], and ATX is the only factor known to exhibit lysoPLD activity in the serum [9]. In sera from heterozygous ATX-null mice, both lysoPLD activity and LPA concentrations were about half of those observed in sera from wild-type mice, showing that ATX is responsible for the bulk of LPA production in the serum [12,13]. On the other hand, when ATX-depleted human [14], mouse [12], or bovine [15] serum was prepared using immunoprecipitation with an anti-ATX monoclonal antibody, the lysoPLD activity was

* Corresponding author at: Department of Clinical Laboratory Medicine, Graduate School of Medicine, The University of Tokyo, 7-3-1 Hongo, Bunkyo-ku, Tokyo 113-8655, Japan. Tel.: +81 3 3815 5411; fax: +81 3 5689 0495.
E-mail address: ikeda-1im@h.u-tokyo.ac.jp (H. Ikeda).

0009-8981/$ – see front matter © 2011 Elsevier B.V. All rights reserved.
doi:10.1016/j.cca.2011.03.014

negligible in ATX-depleted serum, indicating that ATX fully accounts for serum lysoPLD activity [14,15]. In line with these findings, a strong correlation between serum ATX activity and plasma LPA level was observed in human [16] and in mice [17]. Considering the importance of ATX as an enzyme that exerts lysoPLD activity and produces LPA, the measurement of serum ATX concentrations was deemed important. In fact, we previously reported that the lysoPLD enzymatic activity assay was promising for laboratory testing [18].

To date, we have been focusing on a potential role of LPA in (patho)physiology of the liver, and we showed that LPA stimulates the proliferation [19] and contractility [20,21] of hepatic stellate cells, a key player in liver fibrogensis. This evidence prompted us to examine whether LPA and ATX were pathophysiologically involved in liver fibrosis. During an experiment to clarify this point, we found that plasma LPA level and serum ATX activity increased in parallel with liver fibrosis in human [16], and in rats [17].

Recently, ATX immunoenzymetric system has been developed [22], which needs much less time to obtain the results compared to ATX activity assay. Using this assay, serum ATX level has been shown to be strongly correlated with serum ATX activity in healthy subjects and in patients with chronic liver disease, with higher levels observed in female than in male [22]. In this study, we examined whether serum ATX level could be useful as a marker of liver fibrosis in the clinical setting.

2. Patients and methods

2.1. Patients

All the enrolled patients had chronic liver disease caused by hepatitis C virus (HCV; C-CLD), defined as having persistent liver damage for >6 months, serum anti-HCV antibody positivity and a detectable HCV RNA level. Patients with the following conditions were excluded from the study: double infection with both HBV and HCV, the presence of other causes of liver disease, including alcoholism (≥80 g of ethanol daily for at least 5 y) and hepatocellular carcinoma.

ATX level was first examined in stored serum samples of C-CLD patients ($n=74$) with histological analysis of the liver, which were collected between January 1994 and December 2002 with informed consent at the Department of Gastroenterology, University of Tokyo Hospital, Tokyo, Japan.

Furthermore, 134 patients with C-CLD among patients who were seen in the Department of Gastroenterology, University of Tokyo Hospital, between April 2007 and August 2009 were also enrolled. These patients underwent a liver stiffness measurement and were without active liver damage with >100 U/l of alanine aminotransferase (ALT) and cardiac insufficiency, because liver stiffness value has been shown to be unreliable to predict the degree of liver fibrosis in those conditions [23–25].

This study was carried out in accordance with the ethical guidelines of the 1975 Declaration of Helsinki and was approved by the Institutional Research Ethics Committee of the Faculty of Medicine of the University of Tokyo. Informed consent from the patients was obtained for the use of the serum samples.

2.2. Measurement of ATX activity

ATX activity was measured as lysophospholipase D activity using an enzymatic photometric method with the determination of the choline level after the addition of the substrate lysophosphatidylcholine, as previously described [9].

2.3. Measurement of ATX antigen

Serum ATX antigen concentration was determined using a specific 2-site enzyme immunoassay, as previously described, in which the within-run and between-run CVs were 3.1−4.6% and 2.8–4.6%, respectively [22].

Table 1
Characteristics of patients.

Variables	A retrospective cohort	A cohort analyzed with liver stiffness
Age (y)	63 ± 9	67 ± 10
Male/female	42/32	59/75
AST (U/l)	76.5 ± 39.3	44.4 ± 22.4
Platelet count ($\times 10^4/\mu l$)	11.5 ± 4.3	14.2 ± 6.1
Serum ATX level (mg/l)	2.40 ± 0.96	2.20 ± 1.22
Serum hyaluronic acid level (ng/ml)	198.6 ± 200.2	194.1 ± 235.3
Fibrosis stage		
Male F0 & F1/F2 & F3/F4	1/25/16	NA
Female F0 & F1/F2 & F3/F4	2/10/20	NA
Liver stiffness value (kPa)	NA	11.6 ± 8.8
Male ≤7.65/7.65<, ≤13.01/13.01<	NA	27/14/18
Female ≤7.65/7.65<, ≤13.01/13.01<	NA	37/11/27

Values are expressed as the mean ± SD.
NA, not available.

2.4. Histological staging

Liver biopsy was performed under sonography, in which a Tru-cut needle (14-gauge) under sonography was used to obtain an enough hepatic tissue. The samples were all at least 10 mm in length. Fibrosis stage, determined according to the METAVIR group scoring system, was classified as F0, no fibrosis; F1, portal fibrosis without septa; F2, few septa; F3, numerous septa without cirrhosis; or F4, cirrhosis.

2.5. Measurement of liver stiffness

Liver stiffness was measured using transient elastography (FibroScan 502; EchoSens, Paris, France), as described previously [26–28]. Briefly, the measurements were performed in the right lobe of the liver through the inter-costal spaces with the patient lying in the dorsal decubitus position. Liver stiffness measurement was considered valid only when at least ten acquisitions were successful with a success rate of at least 60% and the ratio of inter-quartile range to the median value was larger than 30%. Liver stiffness value was expressed in kilopascals (kPa).

2.6. Statistical analysis

The correlation between two groups, in which the data points were distribution-free, was analyzed using Spearman's rank correlation coefficient. Trends of serum ATX levels in accordance with

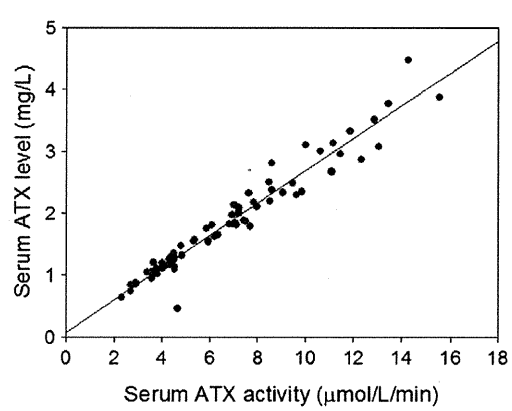

Fig. 1. Correlation of serum ATX level with serum ATX activity in patients with C-CLD. Data from 68 patients were used to analyze a correlation between serum ATX level and serum ATX activity.

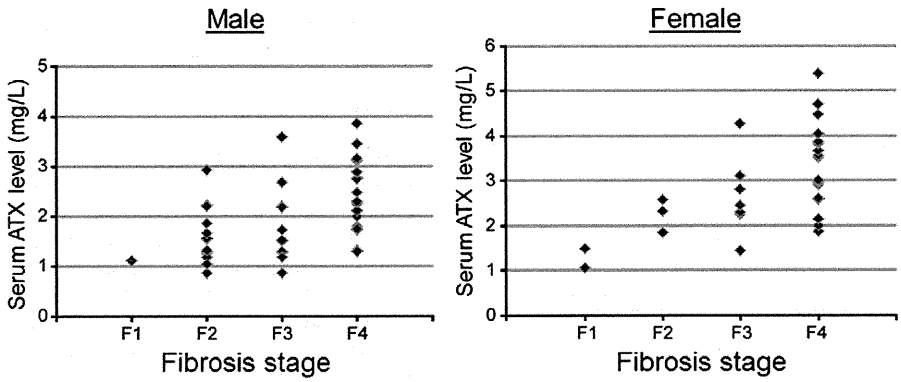

Fig. 2. Correlations of serum ATX level with liver fibrosis stage in male and female patients with C-CLD. Data from 42 male patients and 32 female patients were used to analyze a correlation between serum ATX level and liver fibrosis stage.

fibrosis stage were assessed with the Jonckeere–Terpstra test. A two-sided *P*-value less than 0.05 was considered statistically significant. Statistical procedures were performed using SAS, ver 9.1 (SAS Institute, Inc., Cary, NC).

3. Results

3.1. Patients

The characteristics of the patients in the retrospective cohort whose serum samples were collected between January 1994 and December 2002, and those in another cohort whose serum samples were collected between April 2007 and August 2009, are summarized in Table 1. There were more patients with advanced fibrosis stage in the retrospective cohort compared to the cohort analyzed with liver stiffness value; approximately half of patients had cirrhosis in the retrospective cohort.

3.2. Relationship between serum ATX level and serum ATX activity in patients with C-CLD

Serum ATX level was recently shown to be strongly correlated with serum ATX activity in healthy subjects [22]. We first examined a correlation between serum ATX level and serum ATX activity in patients with C-CLD. As shown in Fig. 1, a strong correlation between serum ATX level and serum ATX activity ($\rho = 0.971$, $P < 0.001$) was confirmed in 68 patients with C-CLD, in whom both serum ATX level and serum ATX activity were measured [22].

3.3. Performances of serum ATX level for the prediction of liver fibrosis stage

In the retrospective cohort, serum ATX level was significantly correlated with liver fibrosis stage in both male ($P = 0.016$, Jonckheere–Terpstra test) and female ($P = 0.005$), as demonstrated in Fig. 2. Then, the performances of serum ATX level for the prediction of liver fibrosis stage were analyzed in comparison with serum hyaluronic acid level and aspartate aminotransferase-to-platelet ratio index (APRI), an established marker of liver fibrosis [29]. Because serum ATX level exhibits a gender difference [22], we evaluated serum ATX level in both male and female patients. Fig. 3 shows the receiver operator characteristic (ROC) curves for serum ATX level, serum hyaluronic acid level and APRI with regard to the prediction of cirrhosis. Table 2 depicts the area under the ROC curves (AUROCs) for the three parameters. AUROCs of serum ATX level for predicting cirrhosis were 0.756 in male and 0.760 in female, which were better than those of serum hyaluronic acid level or APRI. Because this retrospective cohort had a bias with more patients with advanced liver fibrosis, the performances of the three markers to predict significant fibrosis were not analyzed.

3.4. Performances of serum ATX level for the prediction of liver stiffness value

Then, serum ATX level was further evaluated in another cohort with more patients with mild fibrosis (Table 1). In this recent cohort, liver stiffness value was employed as an indicator for liver fibrosis,

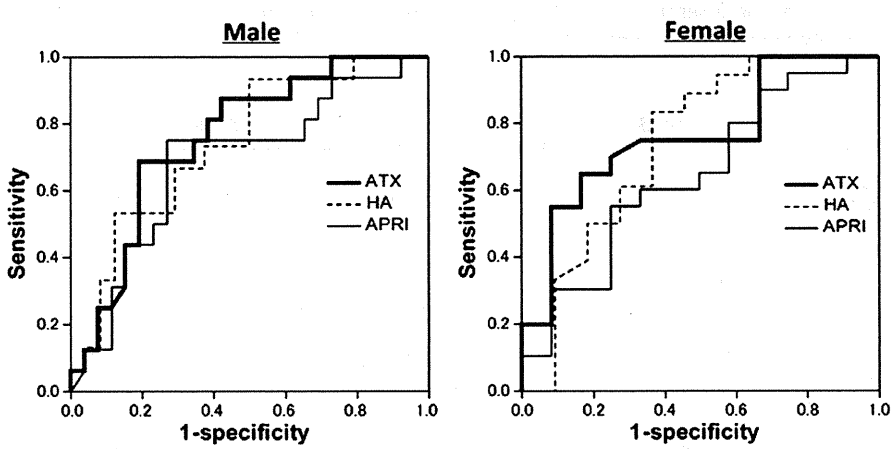

Fig. 3. Receiver operator characteristics (ROC) curves illustrating the relationship between sensitivity and 1 – specificity for serum ATX level, serum hyaluronic acid level, and APRI for discriminating cirrhosis in male and female C-CLD patients. Data from 42 male patients and 32 female patients were used in the ROC statistical analyses comparing the discriminating accuracy of three parameters. HA, hyaluronic acid.

Table 2
Area under the receiver operator characteristic curves (AUROCs) for the three parameters discriminating cirrhosis.

	Parameter	AUROC (95% CI)
Male		
	ATX	0.756 (0.608–0.904)
	HA	0.739 (0.581–0.897)
	APRI	0.686 (0.516–0.857)
Female		
	ATX	0.760 (0.588–0.933)
	HA	0.740 (0.534–0.946)
	APRI	0.642 (0.441–0.843)

HA, hyaluronic acid.

because 1) the strict attention to ethical concerns regarding the performance of liver biopsies for the sole purpose of assessing the liver fibrosis stage was paid, and 2) the general reliability of liver stiffness value in the diagnosis of liver fibrosis has been reported based on the evidence that liver stiffness value is strongly correlated with the fibrosis stage, as determined by a liver biopsy [26,30–34]. The significant correlation was observed between serum ATX level and liver stiffness value, as shown in Fig. 4. Spearman's rank correlation coefficients between serum ATX level and liver stiffness value were 0.635 in male patients ($P<0.001$) and 0.638 in female patients ($P<0.001$), respectively.

Then, we analyzed the performances of serum ATX level, serum hyaluronic acid level, and APRI for the prediction of liver stiffness value. Because a previous meta-analysis showed 7.65 kPa to be the lower limit of stage F2 with significant fibrosis and 13.01 kPa to be the lower limit of stage F4 with cirrhosis in the conventional classifications of liver fibrosis [33], the abilities of these 3 parameters to discriminate a liver stiffness of ≤7.65 kPa from a liver stiffness of >7.65 kPa and a liver stiffness of ≤13.01 kPa from a liver stiffness of >13.01 kPa were analyzed. Fig. 5 shows ROC curves for serum ATX level, serum hyaluronic acid level, and APRI with regard to the prediction of >7.65 kPa or 13.01 kPa of liver stiffness value. Table 3 depicts AUROCs for the 3 parameters. To predict >7.65 kPa of liver stiffness value, serum ATX level was the second best parameter both in male and in female. Serum ATX level had a sensitivity of 70.0% and a specificity of 73.1% with 1.36 mg/l in male, and a sensitivity of 86.5% and a specificity of 70.6% with 2.11 mg/l in female for the prediction of >7.65 kPa of liver stiffness value. To predict >13.01 kPa of liver stiffness value in male, serum ATX level was the best parameter, followed by serum hyaluronic acid level, and APRI. In female, however, serum hyaluronic acid level was the best parameter to predict >13.01 kPa of liver stiffness value, followed by APRI and serum ATX level. Serum ATX level had a sensitivity of 82.4% and a specificity of 74.4% with 1.58 mg/l in male, and a sensitivity of 81.5% and a specificity of 77.3% with 2.56 mg/l in female for the prediction of >13.01 kPa of liver stiffness value.

4. Discussion

The current study indicates that serum ATX level was significantly correlated with liver fibrosis stage and liver stiffness value. Then, the performance of serum ATX level in the prediction of cirrhosis was better than serum hyaluronic acid and APRI. Furthermore, serum ATX level was the second-best parameter in male and in female for predicting >7.65 kPa of liver stiffness, a cut-off for significant fibrosis by meta-analysis [33] and the best parameter in male and the third-best parameter in female for predicting >13.01 kPa of liver stiffness, a cut-off for cirrhosis by meta-analysis [33]. Collectively, serum ATX level may be a useful marker of liver fibrosis, comparable with serum hyaluronic acid. When compared to APRI, serum ATX level may be comparable in female patients and better in male patients as a liver fibrosis marker. Of note, a gender-dependent difference in serum ATX level needs to be taken into consideration when using it as a marker of liver fibrosis.

Because the retrospective cohort analyzed with liver fibrosis stage was smaller and had a bias with more patients with advanced liver fibrosis, serum ATX level was further evaluated in another cohort with more patients with mild fibrosis. In this cohort, we rather chose to employ liver stiffness value as an indicator for liver fibrosis because of ethical considerations. Transient elastography has been shown a reliable tool for assessing liver fibrosis [26,30–34]. According to a previous study for which liver biopsy data was available, serum hyaluronic acid level was effective for discriminating significant fibrosis, with an AUROC of 0.85, and for discriminating cirrhosis, with an AUROC of 0.81, in C-CLD patients [35]. Of note, the AUROC for the serum hyaluronic acid level was 0.814 in male and 0.875 in female for the discrimination of a liver stiffness of ≤7.65 kPa from a liver stiffness of >7.65 kPa, i.e., significant fibrosis, and 0.859 in male and 0.901 in female for the discrimination of a liver stiffness of ≤13.01 kPa from a liver stiffness of >13.01 kPa, i.e., cirrhosis, in the current study. These results were comparable to previous data, suggesting that our current analysis is similarly reliable, compared with studies based on liver histology.

ATX mRNA expression has been predominantly found in brain, lung, duodenum and adrenals and also determined in liver, skeletal muscle, heart at a substantial level [36], suggesting that ATX transcript is expressed in many tissues or organs. Although a regulatory mechanism of ATX expression in various organs has not been clarified yet, we previously demonstrated that serum ATX activity is increased in liver fibrosis, which let us examine whether ATX production might be increased in the liver. As a result, ATX mRNA expression in the liver was not increased in a carbon tetrachloride-induced rat model of liver

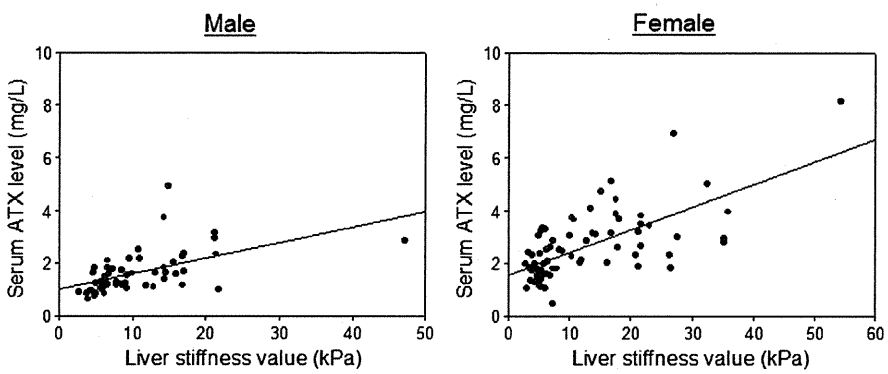

Fig. 4. Correlations of serum ATX level with liver stiffness value in male and female patients with C-CLD. Data from 59 male patients and 75 female patients were used to analyze a correlation between serum ATX level and liver stiffness value.

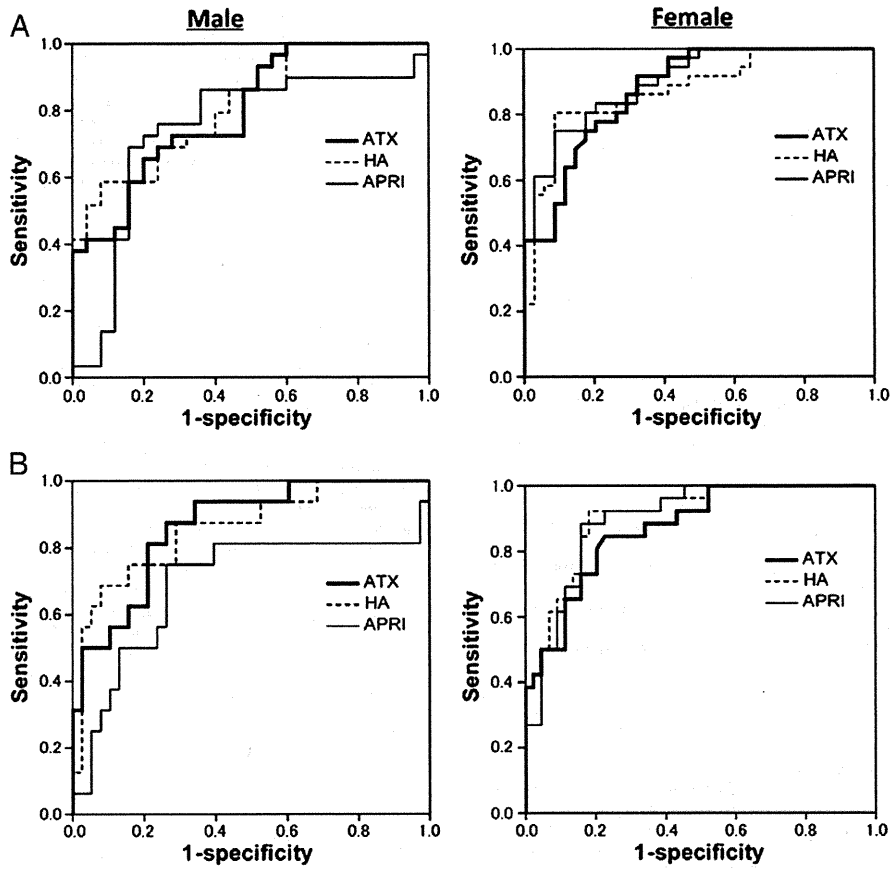

Fig. 5. Receiver operator characteristics (ROC) curves illustrating the relationship between sensitivity and 1 – specificity for serum ATX level, serum hyaluronic acid level, and APRI for discriminating ≤7.65 kPa of liver stiffness from >7.65 kPa of liver stiffness (A) or ≤13.01 kPa of liver stiffness from >13.01 kPa of liver stiffness (B) in male and female C-CLD patients. Data from 59 male patients and 75 female patients were used in the ROC statistical analyses comparing the discriminating accuracy of three parameters. HA, hyaluronic acid.

fibrosis, suggesting that the mechanism of the increase of serum ATX activity might involve the reduction of ATX clearance in the liver [16]. The evidence of early rise in serum ATX activity at 3 h after 70% hepatoctemy in rats is in line with this speculation [16]. In fact, recent evidence indicates that sinusoidal endothelial cells specifically take up ATX in the blood [37]. Therefore, the uptake of ATX by sinusoidal endothelial cells explains, at least in part, the usefulness of serum ATX level as a marker of liver fibrosis. Of interest, sinusoidal endothelial cells also take up hyaluronic acid [38]. However, the kinetics of ATX and hyaluronic acid in the blood are distinctly different: serum ATX level exhibits a gender difference [22], but serum hyaluronic acid level does not. Severely impaired renal function leads to an increase in serum hyaluronic acid level [39,40] but not in serum ATX level [41]. Furthermore, the diet affects serum hyaluronic acid level [42] but not serum ATX level. These points can be advantage of serum ATX level over serum hyaluronic acid level as a liver fibrosis marker. Another advantage of serum ATX level is that serum hyaluronic acid level is increased in patients with chronic inflammation [43], but not serum ATX level [44], suggesting that serum ATX level may be more specific marker of liver fibrosis than serum hyaluronic acid level.

Table 3
Area under the receiver operator characteristic curves (AUROCs) for the three parameters discriminating various liver stiffness categories.

Category of liver stiffness	Parameter	AUROC (95% CI)
≤7.65 kPa *vs.* >7.65 kPa		
Male	ATX	0.799 (0.683–0.914)
	HA	0.814 (0.703–0.924)
	APRI	0.741 (0.596–0.886)
Female	ATX	0.876 (0.798–0.955)
	HA	0.875 (0.792–0.958)
	APRI	0.900 (0.831–0.968)
≤13.01 kPa *vs.* >13.01 kPa		
Male	ATX	0.863 (0.762–0.965)
	HA	0.859 (0.746–0.971)
	APRI	0.689 (0.509–0.870)
Female	ATX	0.872 (0.791–0.953)
	HA	0.901 (0.830–0.973)
	APRI	0.899 (0.827–0.970)

HA, hyaluronic acid.

Regarding APRI, the performance for diagnosing cirrhosis was worst among the three parameters both in male and female and the performance for predicting liver stiffness was also worst in male. This poorer performance of APRI for predicting liver fibrosis and liver stiffness especially in male patients with C-CLD was unexpected [45]. Because the previous analyses of APRI as a marker of liver fibrosis were mainly performed in patients in US and Europe [45], ethnic differences might explain the distinct performances of APRI for predicting cirrhosis and liver stiffness. Nonetheless, APRI as a marker of liver fibrosis should be carefully applied, at least in Japanese male patients with C-CLD.

Our current evidence may shed a light on novel clinical significance of ATX; serum ATX level increases correlatively with liver fibrosis and is useful as its marker. A further study is needed to clarify a potential pathophysiological role of ATX in liver fibrosis as a regulator of plasma LPA level.

List of abbreviations

ATX	autotaxin
LPA	lysophosphatidic acid
lysoPLD	lysophospholipase D
C-CLD	chronic liver disease caused by hepatitis C virus
HCV	hepatitis C virus
ALT	alanine aminotransferase
APRI	aspartate aminotransferase-to-platelet ratio index
ROC	receiver operator characteristic
AUROC	area under the receiver operator characteristic curve

Acknowledgement

This work was supported by the Japanese Society of Laboratory Medicine Fund for the Promotion of Scientific Research (to H.I.).

References

[1] Moolenaar WH. Lysophospholipids in the limelight: autotaxin takes center stage. J Cell Biol 2002;158:197–9.
[2] Moolenaar WH, van Meeteren LA, Giepmans BN. The ins and outs of lysophosphatidic acid signaling. Bioessays 2004;26:870–81.
[3] Mills GB, Moolenaar WH. The emerging role of lysophosphatidic acid in cancer. Nat Rev Cancer 2003;3:582–91.
[4] Hama K, Aoki J, Fukaya M, et al. Lysophosphatidic acid and autotaxin stimulate cell motility of neoplastic and non-neoplastic cells through LPA1. J Biol Chem 2004;279:17634–9.
[5] Xu Y, Shen Z, Wiper DW, et al. Lysophosphatidic acid as a potential biomarker for ovarian and other gynecologic cancers. Jama 1998;280:719–23.
[6] Siess W. Athero- and thrombogenic actions of lysophosphatidic acid and sphingosine-1-phosphate. Biochim Biophys Acta 2002;1582:204–15.
[7] Aoki J, Taira A, Takanezawa Y, et al. Serum lysophosphatidic acid is produced through diverse phospholipase pathways. J Biol Chem 2002;277:48737–44.
[8] Tokumura A, Majima E, Kariya Y, et al. Identification of human plasma lysophospholipase D, a lysophosphatidic acid-producing enzyme, as autotaxin, a multifunctional phosphodiesterase. J Biol Chem 2002;277:39436–42.
[9] Umezu-Goto M, Kishi Y, Taira A, et al. Autotaxin has lysophospholipase D activity leading to tumor cell growth and motility by lysophosphatidic acid production. J Cell Biol 2002;158:227–33.
[10] Stracke ML, Krutzsch HC, Unsworth EJ, et al. Identification, purification, and partial sequence analysis of autotaxin, a novel motility-stimulating protein. J Biol Chem 1992;267:2524–9.
[11] Yang Y, Mou L, Liu N, Tsao MS. Autotaxin expression in non-small-cell lung cancer. Am J Respir Cell Mol Biol 1999;21:216–22.
[12] Tanaka M, Okudaira S, Kishi Y, et al. Autotaxin stabilizes blood vessels and is required for embryonic vasculature by producing lysophosphatidic acid. J Biol Chem 2006;281:25822–30.
[13] van Meeteren LA, Ruurs P, Stortelers C, et al. Autotaxin, a secreted lysophospholipase D, is essential for blood vessel formation during development. Mol Cell Biol 2006;26:5015–22.
[14] Nakamura K, Takeuchi T, Ohkawa R, et al. Serum lysophospholipase D/autotaxin may be a new nutritional assessment marker: study on prostate cancer patients. Ann Clin Biochem 2007;44:549–56.
[15] Tsuda S, Okudaira S, Moriya-Ito K, et al. Cyclic phosphatidic acid is produced by autotaxin in blood. J Biol Chem 2006;281:26081–8.
[16] Watanabe N, Ikeda H, Nakamura K, et al. Both plasma lysophosphatidic acid and serum autotaxin levels are increased in chronic hepatitis C. J Clin Gastroenterol 2007;41:616–23.
[17] Watanabe N, Ikeda H, Nakamura K, et al. Plasma lysophosphatidic acid level and serum autotaxin activity are increased in liver injury in rats in relation to its severity. Life Sci 2007;81:1009–15.
[18] Nakamura K, Ohkawa R, Okubo S, et al. Measurement of lysophospholipase D/autotaxin activity in human serum samples. Clin Biochem 2007;40:274–7.
[19] Ikeda H, Yatomi Y, Yanase M, et al. Effects of lysophosphatidic acid on proliferation of stellate cells and hepatocytes in culture. Biochem Biophys Res Commun 1998;248:436–40.
[20] Yanase M, Ikeda H, Matsui A, et al. Lysophosphatidic acid enhances collagen gel contraction by hepatic stellate cells: association with rho-kinase. Biochem Biophys Res Commun 2000;277:72–8.
[21] Yanase M, Ikeda H, Ogata I, et al. Functional diversity between Rho-kinase- and MLCK-mediated cytoskeletal actions in a myofibroblast-like hepatic stellate cell line. Biochem Biophys Res Commun 2003;305:223–8.
[22] Nakamura K, Igarashi K, Ide K, et al. Validation of an autotaxin enzyme immunoassay in human serum samples and its application to hypoalbuminemia differentiation. Clin Chim Acta 2008;388:51–8.
[23] Arena U, Vizzutti F, Corti G, et al. Acute viral hepatitis increases liver stiffness values measured by transient elastography. Hepatology 2008;47:380–4.
[24] Lebray P, Varnous S, Charlotte F, Varaut A, Poynard T, Ratziu V. Liver stiffness is an unreliable marker of liver fibrosis in patients with cardiac insufficiency. Hepatology 2008;48:2089.
[25] Sagir A, Erhardt A, Schmitt M, Haussinger D. Transient elastography is unreliable for detection of cirrhosis in patients with acute liver damage. Hepatology 2008;47:592–5.
[26] Castera L, Vergniol J, Foucher J, et al. Prospective comparison of transient elastography, Fibrotest, APRI, and liver biopsy for the assessment of fibrosis in chronic hepatitis C. Gastroenterology 2005;128:343–50.
[27] Ziol M, Handra-Luca A, Kettaneh A, et al. Noninvasive assessment of liver fibrosis by measurement of stiffness in patients with chronic hepatitis C. Hepatology 2005;41:48–54.
[28] Masuzaki R, Tateishi R, Yoshida H, et al. Risk assessment of hepatocellular carcinoma in chronic hepatitis C patients by transient elastography. J Clin Gastroenterol 2008;42:839–43.
[29] Manning DS, Afdhal NH. Diagnosis and quantitation of fibrosis. Gastroenterology 2008;134:1670–81.
[30] Shaheen AA, Wan AF, Myers RP. FibroTest and FibroScan for the prediction of hepatitis C-related fibrosis: a systematic review of diagnostic test accuracy. Am J Gastroenterol 2007;102:2589–600.
[31] Talwalkar JA, Kurtz DM, Schoenleber SJ, West CP, Montori VM. Ultrasound-based transient elastography for the detection of hepatic fibrosis: systematic review and meta-analysis. Clin Gastroenterol Hepatol 2007;5:1214–20.
[32] Obara N, Ueno Y, Fukushima K, et al. Transient elastography for measurement of liver stiffness measurement can detect early significant hepatic fibrosis in Japanese patients with viral and nonviral liver diseases. J Gastroenterol 2008;43:720–8.
[33] Friedrich-Rust M, Ong MF, Martens S, et al. Performance of transient elastography for the staging of liver fibrosis: a meta-analysis. Gastroenterology 2008;134:960–74.
[34] Stebbing J, Farouk L, Panos G, et al. A meta-analysis of transient elastography for the detection of hepatic fibrosis. J Clin Gastroenterol 2010;44:214–9.
[35] Mehta P, Ploutz-Snyder R, Nandi J, Rawlins SR, Sanderson SO, Levine RA. Diagnostic accuracy of serum hyaluronic acid, FIBROSpect II, and YKL-40 for discriminating fibrosis stages in chronic hepatitis C. Am J Gastroenterol 2008;103:928–36.
[36] Stefan C, Gijsbers R, Stalmans W, Bollen M. Differential regulation of the expression of nucleotide pyrophosphatases/phosphodiesterases in rat liver. Biochim Biophys Acta 1999;1450:45–52.
[37] Jansen S, Andries M, Vekemans K, Vanbilloen H, Verbruggen A, Bollen M. Rapid clearance of the circulating metastatic factor autotaxin by the scavenger receptors of liver sinusoidal endothelial cells. Cancer Lett 2009;284:216–21.
[38] Fraser JR, Alcorn D, Laurent TC, Robinson AD, Ryan GB. Uptake of circulating hyaluronic acid by the rat liver. Cellular localization in situ. Cell Tissue Res 1985;242:505–10.
[39] Laurent TC, Lilja K, Brunnberg L, et al. Urinary excretion of hyaluronan in man. Scand J Clin Lab Investig 1987;47:793–9.
[40] Hallgren R, Engstrom-Laurent A, Nisbeth U. Circulating hyaluronate. A potential marker of altered metabolism of the connective tissue in uremia. Nephron 1987;46:150–4.
[41] Nakamura K, Nangaku M, Ohkawa R, et al. Analysis of serum and urinary lysophospholipase D/autotaxin in nephrotic syndrome. Clin Chem Lab Med 2008;46:150–1.
[42] Idobe Y, Murawaki Y, Ikuta Y, Koda M, Kawasaki H. Post-prandial serum hyaluronan concentration in patients with chronic liver disease. Intern Med 1998;37:568–75.
[43] Horslev-Petersen K, Bentsen KD, Engstrom-Laurent A, Junker P, Halberg P, Lorenzen I. Serum amino terminal type III procollagen peptide and serum hyaluronan in rheumatoid arthritis: relation to clinical and serological parameters of inflammation during 8 and 24 months' treatment with levamisole, penicillamine, or azathioprine. Ann Rheum Dis 1988;47:116–26.
[44] Masuda A, Nakamura K, Izutsu K, et al. Serum autotaxin measurement in haematological malignancies: a promising marker for follicular lymphoma. Br J Haematol 2008;143:60–70.
[45] Shaheen AA, Myers RP. Diagnostic accuracy of the aspartate aminotransferase-to-platelet ratio index for the prediction of hepatitis C-related fibrosis: a systematic review. Hepatology 2007;46:912–21.

Apoptosis Signal-Regulating Kinase 1 Inhibits Hepatocarcinogenesis by Controlling the Tumor-Suppressing Function of Stress-Activated Mitogen-Activated Protein Kinase

Hayato Nakagawa,[1] Yoshihiro Hirata,[1] Kohsuke Takeda,[2] Yoku Hayakawa,[1] Takehiro Sato,[2] Hiroto Kinoshita,[1] Kei Sakamoto,[3] Wachiko Nakata,[1] Yohko Hikiba,[3] Masao Omata,[4] Haruhiko Yoshida,[1] Kazuhiko Koike,[1] Hidenori Ichijo,[2] and Shin Maeda[1,5]

The stress-activated mitogen-activated protein kinases (MAPKs), c-Jun NH2-terminal kinase (JNK), and p38 have been implicated in hepatocarcinogenesis. Although the many interrelated functions of JNK and p38 are precisely regulated by upstream signaling molecules, little is known about upstream regulators. We investigated the role of apoptosis signal-regulating kinase 1 (ASK1), a major player in the regulation of JNK and p38 activities, in hepatocarcinogenesis using a mouse hepatocellular carcinoma (HCC) model. ASK1-deficient ($ASK1^{-/-}$) and wildtype (WT) mice were treated with diethylnitrosamine on postnatal day 14. Strikingly, after 7 months, approximately three times as many tumors developed in $ASK1^{-/-}$ mice as in WT mice. Although JNK and p38 activation were attenuated in $ASK1^{-/-}$ HCCs relative to WT HCCs, cell proliferation was comparable in HCCs from both types of mice. On the other hand, both cancer cell apoptosis and hyperphosphorylation of BimEL, a proapoptotic Bcl-2 family member, were suppressed in the $ASK1^{-/-}$ HCCs. $ASK1^{-/-}$ mice showed remarkable resistance to Fas-induced hepatocyte apoptosis *in vivo*, probably because of attenuated JNK-mediated BimEL phosphorylation and mitochondrial apoptotic pathway activation. The reintroduction of ASK1 to $ASK1^{-/-}$ mouse liver using an adenoviral vector restored Fas-induced hepatocyte death and phosphorylation of JNK and BimEL. Similar findings were obtained in tumor necrosis factor alpha-induced hepatocyte apoptosis. Furthermore, ASK1 was involved in DNA damage-induced p21 up-regulation through a p38 pathway. *Conclusion:* ASK1 is involved in death receptor-mediated apoptosis and DNA-damage response by way of stress-activated MAPK in the liver, and thus acts as a tumor suppressor in hepatocarcinogenesis. This study provides new insight into the regulation of stress-activated MAPK signaling in hepatocarcinogenesis. (HEPATOLOGY 2011;54:185-195)

Hepatocellular carcinoma (HCC) is the third most common cause of cancer mortality; thus, understanding the molecular carcinogenic mechanism is an important issue.[1] Several molecular pathways have been reported to play important roles in hepatocarcinogenesis. In particular, clinical and experimental studies have implicated the stress-activated mitogen-activated protein kinase (MAPK) cascades that converge on c-Jun NH_2-

Abbreviations: ALT, alanine aminotransferase; ASK1, apoptosis signal-regulating kinase 1; DEN, diethylnitrosamine; GalN, galactosamine; HCC, hepatocellular carcinoma; JNK, c-Jun NH2-terminal kinase; LPS, lipopolysaccharide; MAPK, mitogen-activated protein kinase; MAP3K, mitogen-activated protein kinase kinase kinase; TNF-α, tumor necrosis factor-α.

From the [1]Department of Gastroenterology, University of Tokyo, Tokyo, Japan; [2]Laboratory of Cell Signaling, Graduate School of Pharmaceutical Sciences, University of Tokyo, Tokyo, Japan; [3]Division of Gastroenterology, Institute for Adult Diseases, Asahi Life Foundation, Tokyo, Japan; [4]Yamanashi Prefectural Hospital Organization, Yamanashi, Japan; [5]Department of Gastroenterology, Yokohama City University, Yokohama, Japan.

Received December 22, 2010; accepted April 2, 2011.

Address reprint requests to: Shin Maeda, Department of Gastroenterology, Yokohama City University, 3-9 Fukuura, Kanazawa-ku, Yokohama, 236-0004, Japan. E-mail: smaeda@med.yokohama-cu.ac.jp; Fax: +81-45-787-2327.

View this article online at wileyonlinelibrary.com.

DOI 10.1002/hep.24357

Additional Supporting Information may be found in the online version of this article.

terminal kinase (JNK) and p38 as key regulators of hepatocarcinogenesis.[2-6]

JNK and p38 have complex functions and modulate a wide range of cellular effects, including apoptosis, proliferation, differentiation, migration, and inflammation.[7] Evidence implicating the JNK and p38 signaling pathways in the development of various types of cancer is strong, although certain cells use these signaling pathways to combat cancer development, whereas others use these pathways as cancer promoters.[8,9] Crosstalk between the JNK and p38 pathways further complicates the roles of these pathways in carcinogenesis.[7] Although determining the mechanisms regulating these complex and multifunctional signaling pathways is essential for the development of new therapeutic approaches, these mechanisms are not yet well understood.

The activities of JNK and p38 are tightly regulated by upstream MAPK kinases and MAPK kinase kinases (MAP3Ks). Acting far upstream in the intracellular MAPK signaling cascade, MAP3Ks respond to intracellular and extracellular stimuli and determine cell fate.[10] Apoptosis signal-regulating kinase 1 (ASK1), a ubiquitously expressed MAP3K, selectively activates the JNK and p38 signaling pathways in response to a variety of stimuli, including reactive oxygen species and cytokines, and has been widely accepted as a major player in the modulation of JNK and p38 activities regulating cell death.[11] In liver disease, ASK1 is involved in acetaminophen-induced acute liver injury.[12] Furthermore, recent reports revealed that ASK1 participates in colon and skin cancer development through the regulation of apoptosis and inflammation.[13,14] However, involvement of ASK1 in hepatocarcinogenesis has not been reported.

In this study we examined whether ASK1 plays a role in hepatocarcinogenesis using a diethylnitrosamine (DEN)-induced mouse HCC model. We found that ASK1 deficiency promoted the development of HCC, and ASK1 inhibited hepatocarcinogenesis by controlling the tumor-suppressing function of stress-activated MAPK.

Materials and Methods

Animals. Male ASK1-deficient ($ASK1^{-/-}$), $JNK1^{-/-}$, $JNK2^{-/-}$, and C57BL/6 wildtype (WT) mice (Clea Japan, Tokyo, Japan) were used in the experiments. $ASK1^{-/-}$, $JNK1^{-/-}$, and $JNK2^{-/-}$ mice were generated as described[12,15] and backcrossed into the C57BL/6 strain at least 14 times. Mice were maintained under conventional conditions under a light/dark cycle.

All of the experimental protocols were approved by the Ethics Committee for Animal Experimentation and conducted in accordance with the National Institutes of Health (NIH) *Guidelines for the Care and Use of Laboratory Animals.*

Drug Administration and Experimental Design in an* In Vivo *Model. In the DEN-induced HCC model, DEN (Sigma, St. Louis, MO) dissolved in phosphate-buffered saline (PBS) was injected intraperitoneally into mice (25 mg/kg) on postnatal day 14. Mice were sacrificed after 7 months and their livers were removed and examined for visible tumors. In the DEN-induced acute liver injury model, mice were injected intraperitoneally with 100 mg/kg DEN. In the Fas-induced liver injury model, mice (8-10 weeks old) were injected intraperitoneally with the agonistic anti-Fas antibody Jo2 (0.4 μg/g body weight; BD Pharmingen, CA) dissolved in PBS. In the lipopolysaccharide (LPS)/D-galactosamine (GalN)-induced liver injury model, mice were injected intraperitoneally with LPS (20 μg/kg; Sigma) and GalN (1,000 mg/kg; Wako). Some mice were pretreated with JNK inhibitor SP600125 (25 mg/kg; Biomol, PA) or p38 inhibitor SB203580 (25 mg/kg; Wako, Osaka, Japan) dissolved in PBS containing 10% dimethyl sulfoxide. Inhibitors were administered intraperitoneally 1 hour before Jo2 or DEN injection. Histological analyses, RNA extraction, real-time polymerase chain reaction (PCR), and generation of bone marrow chimeric mice were performed as described in the Supporting Information.

Cells and RNA Interference. The human HCC cell lines HuH7 (Human Science, Tokyo, Japan) and PLC/PRF/5 (Riken, Tsukuba, Japan) and a human normal hepatocyte line (ACBRI, Kirkland, WA) were cultured in Dulbecco's modified Eagle medium supplemented with 10% fetal bovine serum. Cell numbers were determined using a Cell Counting Kit-8 (Dojindo Laboratories, Kumamoto, Japan). RNA oligonucleotides were synthesized by Qiagen (Hilden, Germany), and small interfering RNA (siRNA) transfections were performed using RNAiMAX (Invitrogen, Carlsbad, CA). Ultraviolet (UV) irradiation was performed using a UVB lamp (UVP, Upland, CA).

Immunoblotting and Coimmunoprecipitation Analysis. Details are described in the Supporting Information. Anti-ASK1 and anti-phospho-ASK1 antibodies were as described.[16,17]

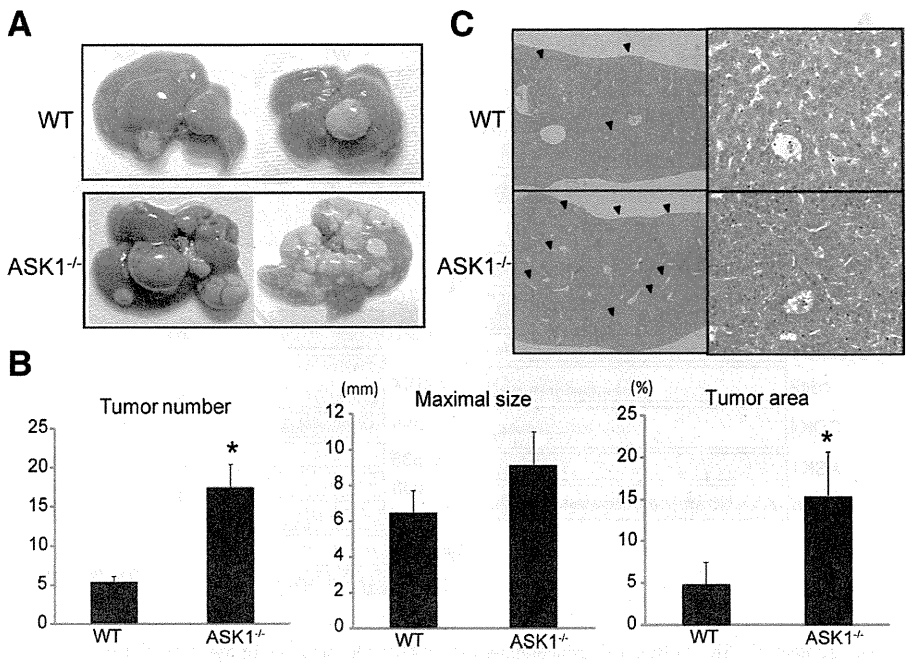

Fig. 1. Increased HCC development in ASK1$^{-/-}$ mice. (A) Livers from 7-month-old DEN-treated WT and ASK1$^{-/-}$ mice. (B) Tumor numbers, maximal tumor sizes, and tumor-occupied areas in WT and ASK1$^{-/-}$ mouse livers. Data are expressed as means ± standard error of the mean (SEM) (WT, n = 14; ASK1$^{-/-}$, n = 12). *$P < 0.05$, compared with WT mice. (C) Typical histological appearance of livers (left) and HCCs (right) from DEN-treated WT and ASK1$^{-/-}$ mice (hematoxylin and eosin [H&E] staining).

Infection of Recombinant Adenovirus. Recombinant adenoviruses encoding β-galactosidase (LacZ) and HA-tagged ASK1 (Ad-ASK1) were constructed as described.[18] Adenoviruses were diluted in PBS and injected into the tail vein 48 hours before Jo2 administration (1×10^8 plaque-forming units [PFU]/mouse).

Statistical Analyses. Statistical analyses were performed using Student's t test or analysis of variance (ANOVA), followed by Dunnett's test where appropriate. $P < 0.05$ was considered statistically significant.

Results

Loss of ASK1 Accelerates Chemically Induced Hepatocarcinogenesis. To determine the role of ASK1 in hepatocarcinogenesis, male WT and ASK1$^{-/-}$ mice were injected with 25 mg/kg DEN on postnatal day 14. After 7 months, untreated WT and ASK1$^{-/-}$ mice revealed no spontaneous liver dysfunction or tumor formation, whereas all mice given DEN developed typical HCCs. Strikingly, the number of detectable tumors was approximately three times higher in ASK1$^{-/-}$ mice than in WT mice, and the tumor-occupied areas were also more extensive in ASK1$^{-/-}$ mice than in WT mice (Fig. 1B,C). The maximum tumor size tended to be larger in ASK1$^{-/-}$ mice, but the difference was not statistically significant (Fig. 1B). DEN-induced liver tumors were histologically similar to well-to-moderately differentiated human HCCs, and the pathological characteristics of the tumors from WT and ASK1$^{-/-}$ mice were similar (Fig. 1C). Thus, loss of ASK1 accelerated DEN-induced HCC development.

Role of ASK1 in Cancer Cell Proliferation and Apoptosis. We compared the characteristics of DEN-induced HCCs in WT and ASK1$^{-/-}$ mouse livers. The phosphorylation level of JNK, but not of p38, was higher in HCCs than in nontumor tissues, and JNK and p38 phosphorylation levels were lower in ASK1$^{-/-}$ HCCs than in WT HCCs (Fig. 2A). However, important downstream substrates of stress-activated MAPK involved in cell-cycle and tumor promotion, such as c-Jun and cyclin D1, were expressed at comparable levels in WT and ASK1$^{-/-}$ mice (Fig. 2A). Additionally, the frequency of cells positive for proliferating cell nuclear antigen (PCNA), a marker of cell proliferation, was similar for the WT and ASK1$^{-/-}$ HCCs (Fig. 2B). Because ASK1 appeared to be expressed at slightly higher levels in HCCs than in nontumor tissues (Fig. 3A), we examined whether ASK1 affects cancer cell proliferation *in vitro* by treating the HCC cell line HuH7 with ASK1-specific siRNA. ASK1-silencing decreased JNK phosphorylation (but not p38 phosphorylation) and c-Jun expression, decreased cyclin D1 expression slightly, and inhibited cell proliferation slightly (Fig. 3C,D), suggesting that the ASK1–JNK pathway weakly enhances HCC cell proliferation. A similar result was also observed in the PLC/PRF/5 HCC cell line (Fig. 3D). However, as discussed above, the WT

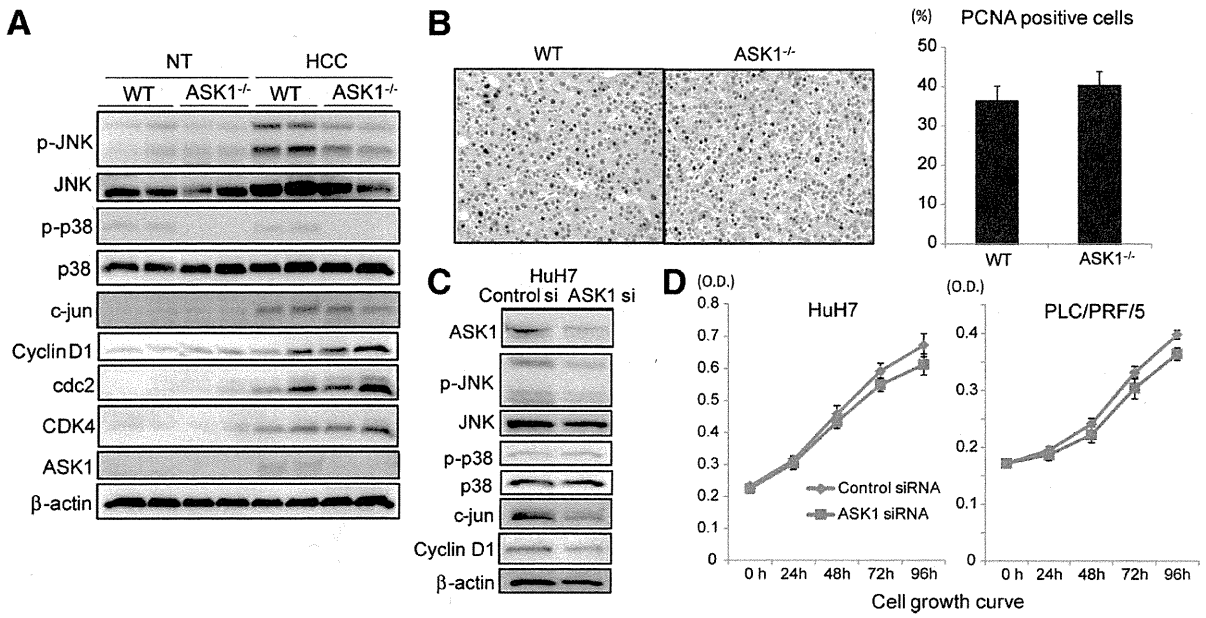

Fig. 2. Role of ASK1 in HCC cell proliferation. (A) Western blot analysis of the indicated proteins in nontumor (NT) and HCC liver tissues from WT and ASK1$^{-/-}$ mice. β-Actin was used as a loading control. (B) Representative PCNA staining of WT and ASK1$^{-/-}$ HCC tissue sections. Bar graph showing frequencies of PCNA-positive cells. Data are expressed as means ± SEM (n = 9 per group). (C) Expression levels of indicated proteins in HuH7 cells 48 hours after transfection with ASK1 or control siRNA. (D) Numbers of HuH7 and PLC/PRF/5 cells counted after transfection. Data are plotted as means ± standard deviation (SD).

and ASK1$^{-/-}$ HCCs exhibited similar c-Jun expression and cell proliferation rates *in vivo*, suggesting that other compensatory pathways promote c-Jun expression and cell proliferation in ASK1$^{-/-}$ HCCs. Based on these results, we conclude that the loss of ASK1 does not promote cancer cell proliferation and that there are other reasons for accelerated hepatocarcinogenesis in ASK1$^{-/-}$ mice.

Next, we compared the numbers of apoptotic cells in the WT and ASK1$^{-/-}$ mice livers using the

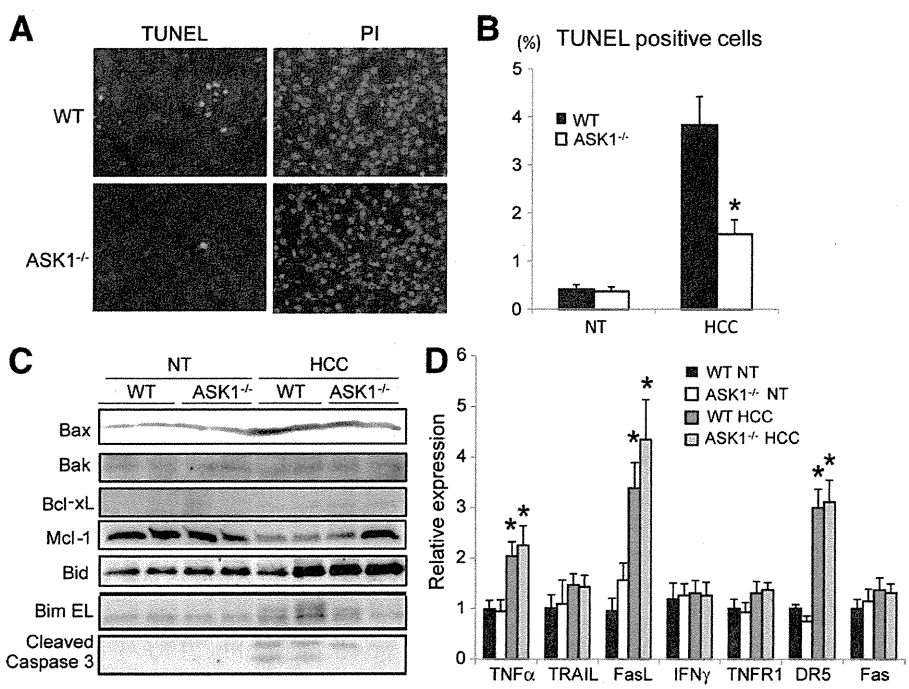

Fig. 3. Apoptosis is suppressed in ASK1$^{-/-}$ HCC tissues. (A) Representative TUNEL-stained sections of HCC tissues from WT and ASK1$^{-/-}$ mice. (B) Frequencies of TUNEL-positive apoptotic cells in nontumor and HCC liver tissues. Data are expressed as means ± SEM (n = 9 per group). *P < 0.05, compared with HCC tissue from WT mice. (C) Western blot analysis of the indicated proteins in nontumor and HCC liver tissue from WT and ASK1$^{-/-}$ mice. (D) Relative mRNA levels for death ligands and receptors in nontumor and HCC liver tissues from WT and ASK1$^{-/-}$ mice determined by real-time PCR. Data are expressed as means ± SEM (n = 9 per group). *P < 0.05, compared with nontumor tissue from WT mice.

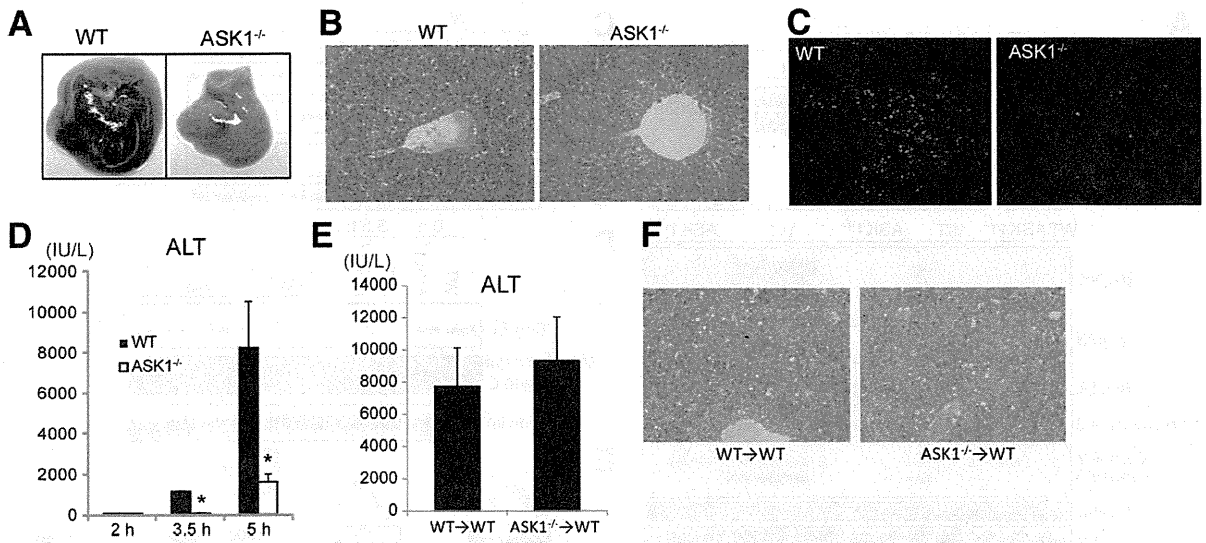

Fig. 4. Involvement of ASK1 in Fas-induced hepatocyte apoptosis. Mice were injected intraperitoneally with the anti-Fas antibody Jo2 (0.4 μg/g). (A) Representative images of WT and ASK1$^{-/-}$ mouse livers 5 hours posttreatment. (B) Histological images of H&E-stained liver obtained 5 hours posttreatment. (C) TUNEL-stained liver sections from WT and ASK1$^{-/-}$ mice taken 5 hours posttreatment. (D) Serum ALT levels 2, 3.5, and 5 hours posttreatment. Data are expressed as means ± SEM (n = 3 per group at 2 hours; n = 5 per group at 3 and 5 hours). *$P <$ 0.05, compared with WT mice. (E,F) Analysis of the role of ASK1 in hematopoietic cells in Fas-induced liver injury. (E) Serum ALT levels 5 hours after Jo2 administration to bone marrow-chimeric mice. WT mice were transplanted with WT or ASK1$^{-/-}$ mouse-derived bone marrow cells. Data are expressed as means ± SEM (n = 5 per group). (F) Histological image of H&E-stained liver obtained 5 hours after Jo2 administration.

terminal deoxynucleotidyl transferase-mediated dUTP nick end labeling (TUNEL) assay. As shown in Fig. 3A,B, significantly fewer apoptotic tumor cells were found in ASK1$^{-/-}$ HCCs than in WT HCCs. Consistent with this, caspase-3 activation was significantly attenuated in ASK1$^{-/-}$ HCCs (Fig. 3C). Messenger RNA (mRNA) levels for the death ligands tumor necrosis factor-α (TNF-α) and FasL and the death receptor TRAIL-R2/DR5 were higher in HCCs than in nontumor tissues, but did not differ significantly between WT and ASK1$^{-/-}$ HCCs (Fig. 3D). These findings indicate that death receptor pathways were activated in DEN-induced HCC tissues, but ASK1 does not regulate the expression of the main modulators. Furthermore, the expression levels of Bcl-2 families were almost identical in WT and ASK1$^{-/-}$ mice, as shown by western blot analysis (Fig. 3C). However, slower migration of the proapoptotic Bcl-2 family member BimEL band, indicating hyperphosphorylation of BimEL, was more predominant in WT HCCs than with ASK1$^{-/-}$ HCCs (Fig. 3C). JNK-mediated Bim phosphorylation has been reported to play an important role in death receptor-mediated apoptosis in the liver,[19,20] and defective death receptor signaling is considered to be a cause of tumor immune escape.[21] Based on these results, we hypothesized that the loss of ASK1 might accelerate hepatocarcinogenesis by allowing cells to escape death receptor-mediated apoptosis.

ASK1 Is Involved in Fas-Induced Hepatocyte Apoptosis. To evaluate whether ASK1 plays a role in Fas-mediated hepatocyte apoptosis, WT and ASK1$^{-/-}$ mice were injected intraperitoneally with agonistic anti-Fas antibody (Jo2), which causes severe liver damage through apoptotic Fas signaling. Because a recent report showed that the death pathway in hepatocytes loses its dependence on mitochondria when the cells are cultured on plates,[22] we assessed the role of ASK1 in Fas-mediated apoptosis using an *in vivo* model. As shown in Fig. 4A, the liver from WT mice turned dark red at 5 hours after injection, which was indicative of widespread hemorrhage. In contrast, the liver from ASK1$^{-/-}$ mice showed only slight reddening. The histological examination revealed extensive hepatic apoptosis and hemorrhage in WT mice, but only focal apoptotic change in ASK1$^{-/-}$ mice (Fig. 4B,C). Consistent with these observations, serum alanine aminotransferase (ALT) levels in ASK1$^{-/-}$ mice were significantly lower than those in WT mice (Fig. 4D).

On the other hand, secondary inflammatory responses have been reported to modulate Jo2-induced liver injury.[23] To rule out the possibility that ASK1 may be involved in Jo2-induced secondary inflammatory responses, we performed Jo2-induced liver injury experiments using bone marrow chimeric mice. WT mice transplanted with ASK1$^{-/-}$ or WT mouse-

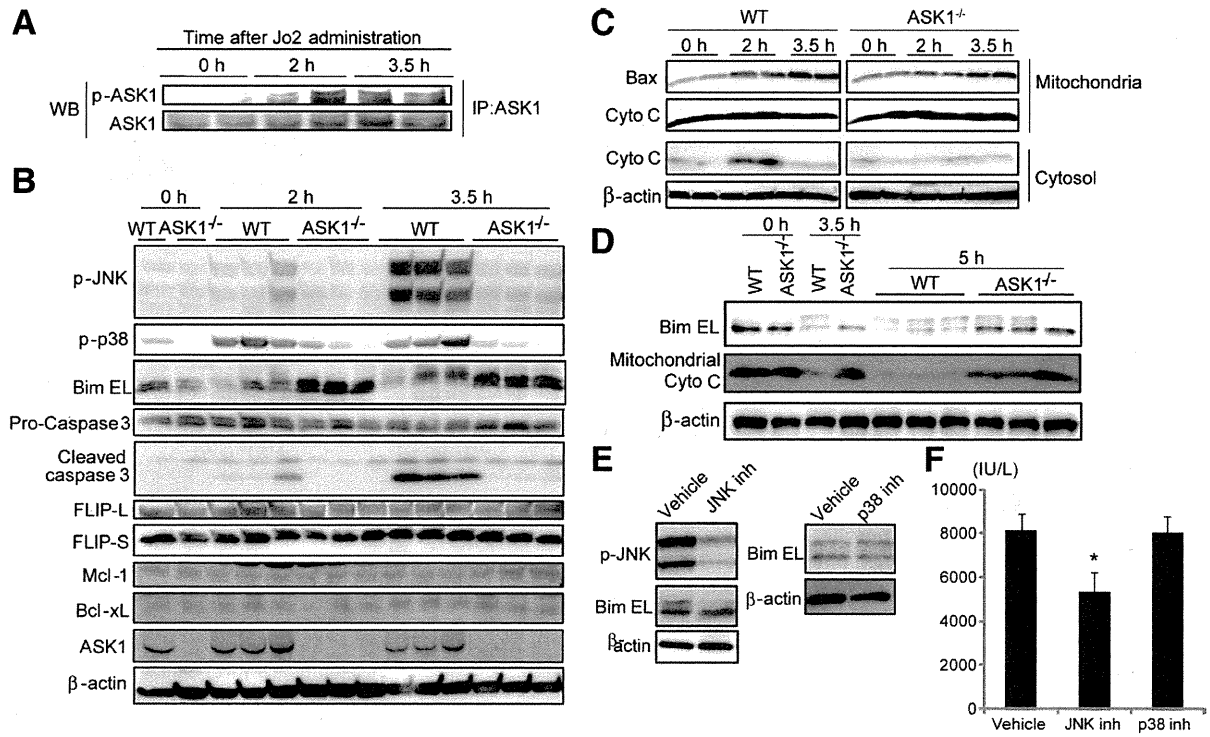

Fig. 5. Analysis of the Fas-signaling pathway. (A) ASK1 activation in WT mouse liver after Jo2 injection. Total liver lysates were immunoprecipitated with ASK1 antibody and analyzed for ASK1 activation by immunoblotting with antibody specific for phospho-ASK1. (B) Western blot analysis of the indicated proteins in WT and ASK1$^{-/-}$ mouse liver. (C) Western blot analysis of Bax and cytochrome *c* in the cytosolic and mitochondrial fractions of WT and ASK1$^{-/-}$ mouse liver. (D) Western blot analysis of BimEL in total liver lysates and of cytochrome *c* in mitochondrial liver fractions from WT and ASK1$^{-/-}$ mice 5 hours after Jo2 administration. (E) Effect of JNK inhibitor and p38 inhibitor on Fas-induced BimEL phosphorylation. (F) Bar graph shows serum ALT levels 5 hours after Jo2 administration to mice pretreated with vehicle, JNK inhibitor, or p38 inhibitor. Data are expressed as means ± SEM (n = 5 per group). *$P < 0.05$, compared with vehicle-treated mice.

derived bone marrow cells showed similar extents of liver injury after Jo2 injection (Fig. 4E,F). These results suggest that ASK1 is involved in Fas-mediated direct hepatocyte apoptosis.

ASK1 Is Required for Activation of the JNK-Bim Pathway in Fas-Induced Apoptotic Signaling. We observed ASK1 phosphorylation after Jo2 administration in WT mouse liver, suggesting that ASK1 was activated in Fas signaling *in vivo* (Fig. 5A). Expression levels of antiapoptotic proteins which have been reported to be implicated in Fas-induced liver injury were not affected by the absence of ASK1 (Fig. 5B). On the other hand, Jo2-induced JNK, p38, and caspase-3 activations were significantly attenuated in ASK1$^{-/-}$ mice compared with WT mice (Fig. 5B).

Bim is phosphorylated by JNK and subsequently cleaved by caspase-3, and becomes a hyperactive inducer of cytochrome *c* release, leading a positive amplification loop in apoptosis.[24,25] In western blot analysis of liver proteins, Jo2 injection induced slower migration of the BimEL band in WT mice, whereas the change in BimEL migration was significantly attenuated in ASK1$^{-/-}$ mice, as also seen in HCC tissues (Fig. 5B). Additionally, we analyzed the activation of the mitochondrial apoptotic pathway, which is essential for Fas-induced apoptosis of hepatocytes (so-called type II cells). The mitochondrial Bax translocation was slightly lower and the cytosolic release of cytochrome *c* was significantly reduced in ASK1$^{-/-}$ mice compared with WT mice at 2 and 3.5 hours after Jo2 administration (Fig. 5C). At 5 hours after Jo2 administration, marked phosphorylation and subsequent degradation of BimEL and reduction of the cytochrome *c* level in the mitochondrial fraction were seen in WT mice, whereas these changes were significantly suppressed in ASK1$^{-/-}$ mice (Fig. 5D). As reported,[19] administration of a JNK inhibitor reduced Jo2-induced BimEL phosphorylation and serum ALT elevation. However, administration of a p38 inhibitor had no detectable effect on BimEL phosphorylation or liver injury (Fig. 5E,F). These results suggest that ASK1 plays an important role in Fas-induced activation of the JNK–Bim–mitochondrial apoptotic pathway.